electricity

MDPI

Article

Optimal Allocation and Sizing of BESS Based on a Reliability-Oriented Planning Approach for Transmission Systems

Sergio David Diaz-Perez [1], Juan Guillermo Marin-Quintero [1], Jorge Ivan Silva-Ortega [1,*], Rafael Peña Gallardo [2], Cesar Augusto Orozco-Henao [3] and Andrés Ricardo Herrera-Orozco [4]

[1] Energy Department, Universidad de la Costa, Barranquilla 080002, Colombia; sdiaz6@cuc.edu.co (S.D.D.-P.); jmarin14@cuc.edu.co (J.G.M.-Q.)
[2] Facultad de Ingeniería, Universidad Autónoma de San Luis Potosí, Manuel Nava 8, Zona Universitaria, San Luis Potosí 78290, Mexico; rafael.pena@uaslp.mx
[3] School of Electrical, Electronics and Telecommunications Engineering, Universidad Industrial de Santander, Bucaramanga 680002, Colombia; caorohen@uis.edu.co
[4] Department of Electrical Engineering, Universidad Tecnologica de Pereira, Pereira 660003, Colombia; arherrera@utp.edu.co
* Correspondence: jsilva6@cuc.edu.co

Abstract

Planning battery energy storage systems (BESS) in transmission networks requires accounting for the effects of component failures on supply continuity. This paper proposes a reliability-oriented methodology based on a Mixed Gray Wolf Optimizer (MGWO) to determine BESS locations, rated active power capacities, and technology selection between lithium-ion (Li-ion) and vanadium redox flow (VRF) batteries. The framework incorporates stochastic reliability models for transmission lines, transformers, busbars, and BESS units. The objective is to minimize the equally weighted average of annual energy not supplied (ENS) across single-generator-outage scenarios, subject to technical constraints and an investment budget. BESS sizing refers to rated power in MW; energy capacity and chronological state of charge are not explicitly modeled. The methodology is evaluated using the IEEE 39-bus New England test system with representative hourly demand profiles. Under a maximum investment budget of USD 300 million, the selected solution comprises 338.66 MW of installed BESS capacity, including 280.78 MW of Li-ion storage and 57.88 MW of VRF storage, at a total investment of USD 299.87 million. Relative to the reference case, SAIDI and SAIFI decrease by 13.76% and 13.11%, respectively. During optimization, the fitness value decreases from approximately 0.878 to 0.828 p.u., representing an improvement of about 6.5% relative to the initial solution. Ten independent runs yield final fitness values between 0.8213 and 0.8300 p.u. These results demonstrate the framework's ability to identify feasible BESS configurations that improve reliability under the adopted modeling assumptions.

Keywords: reliability assessment; gray wolf optimization; BESS planning; component outages

Check for updates

Academic Editor: Ottorino Veneri

Received: 31 July 2026
Revised: 21 October 2026
Accepted: 22 October 2026
Published: 3 November 2026

Copyright: © 2026 by the authors. Licensee MDPI, Basel, Switzerland. This article is an open access article distributed under the terms and conditions of the Creative Commons Attribution (CC BY) license.

1. Introduction

1.1. Motivation

In recent years, modern transmission systems have faced increasingly challenging operating conditions due to growing electricity demand, aging infrastructure, and the large-scale integration of renewable energy resources (RES). Among these factors, the widespread deployment of RES has introduced additional uncertainty into system operation because of their intermittent and stochastic nature [1]. Transmission systems are exposed to random

component outages and repair processes that can alter network topology, reduce power transfer capability, and increase the risk of service interruptions, particularly when the system operates near its technical limits [2]. Among the different sources of uncertainty affecting power-system operation, the availability of transmission lines, transformers, substations, generation units, and storage systems is particularly relevant to reliability-oriented planning. Therefore, the allocation and sizing of BESS should consider not only technical and economic criteria but also the stochastic reliability behavior of the storage technologies and network components.

To address these challenges, energy storage systems (ESSs) have emerged as a promising solution for enhancing the reliability, flexibility, and resilience of transmission systems. ESS technologies can be classified into mechanical, thermal, electrical, and electrochemical storage systems. Among these alternatives, electrochemical storage technologies have attracted considerable attention owing to their modularity, scalability, high cycle life, and energy efficiency [3]. In particular, battery energy storage systems (BESS) have become one of the most widely adopted storage technologies in power-system applications due to their fast response capabilities and their ability to absorb or inject active power as required. Although BESS deployment is not limited to transmission systems and has also expanded into distribution networks, its operational flexibility makes it especially valuable for supporting modern power-grid operations [4]. Among the various technologies used in BESS, Li-ion technology is one of the most technologically mature energy storage solutions due to its remarkable energy density and operating voltage, which makes it suitable for ancillary service applications [5].

From a transmission system perspective, BESS can provide multiple operational and reliability-related benefits, including peak-load management, frequency regulation, voltage support, reduced energy not supplied (ENS) during outages, and facilitation of renewable energy integration [6]. Consequently, BESS can act as flexible transmission support resources capable of improving system performance under both short-term disturbances and long-term reliability challenges [7].

Despite these advantages, the effective integration of BESS into transmission systems remains a complex planning problem. The reliability contribution of a storage system depends strongly on factors such as installation location, rated power, availability, and storage technology. An improperly sized or poorly located BESS may result in underutilized resources, limited reliability improvement, and unnecessary investment costs. Furthermore, different BESS technologies exhibit distinct reliability characteristics, including failure rates, availability levels, operational constraints, and response capabilities, which directly influence their effectiveness during critical system conditions [8]. Therefore, BESS planning should not be restricted to determining optimal locations and capacities; it should also account for the reliability behavior of storage technologies and their contribution to overall system performance [9].

Several BESS allocation and sizing studies adopt deterministic formulations focused primarily on technical and economic objectives, such as voltage profile improvement, power-loss reduction, congestion management, frequency support, and operating-cost minimization [10]. These approaches are appropriate for evaluating BESS performance under predefined operating conditions or specified contingency scenarios. However, the subset of deterministic formulations considered in this review does not explicitly incorporate component failure probabilities, repair times, or stochastic outage durations. Consequently, although these formulations can identify technically effective BESS configurations for the analyzed scenarios, they may not directly quantify the expected reliability contribution of the storage system under random component outages. This limitation motivates the incorporation of probabilistic reliability models into the BESS planning problem [9].

In contrast, stochastic reliability assessment provides a more realistic framework for evaluating transmission system performance under uncertainties [11]. By incorporating probabilistic models of failures associated with components such as transmission lines, transformers, substations, and generation units, stochastic approaches enable the quantification of reliability indices and facilitate the evaluation of alternative BESS deployment strategies. Consequently, stochastic modeling enables a more comprehensive assessment of how BESS location, size, technology, and availability affect the ability of the transmission system to maintain supply continuity under critical contingency states [12].

Despite the growing body of research on BESS planning, limited attention has been given to the combined influence of storage technology reliability characteristics and stochastic transmission component outages on BESS allocation and sizing. This gap motivates the development of reliability-oriented planning methodologies that determine BESS locations, technologies, and power capacities to improve system adequacy while accounting for component failures and repair processes.

Accordingly, the proposed framework represents transmission lines, transformers, substation configurations, and BESS units through two-state stochastic reliability models, while generator unavailability is assessed through single-generator-outage scenarios. Demand variation is represented using typical hourly profiles rather than probabilistic load models. Equipment degradation, weather-dependent failures, and stochastic load variations are outside the scope of this study.

1.2. State-of-the-Art

The allocation and sizing of BESS are not limited to transmission system applications. Numerous studies have investigated their deployment in medium- and low-voltage distribution networks, demonstrating improvements in voltage regulation, power-loss reduction, renewable energy integration, and operational flexibility [13–15]. The promising results obtained in transmission systems have motivated the extension of BESS planning methodologies to distribution networks, where storage systems can provide additional benefits related to system adequacy, operational security, and enhanced reliability.

BESS planning studies can be categorized according to their objectives. Some studies focus on determining the optimal location and capacity of storage systems to improve operational performance, including loss minimization, congestion relief, voltage profile enhancement, and frequency support [14,16,17]. Other studies adopt a more comprehensive perspective by simultaneously determining storage allocation, sizing, and technology selection, acknowledging that different battery technologies exhibit distinct technical and economic characteristics. However, reliability characteristics that directly influence system performance such as failures and repair rates are not considered in the optimization formulation [15,18].

Methodologically, BESS planning approaches can generally be classified into deterministic and stochastic frameworks. Deterministic methods assume predefined operating conditions and fixed system parameters, focusing primarily on technical and economic optimization objectives [8,14–17,19–21].

Bio-inspired optimization techniques have also received significant attention due to their ability to solve highly nonlinear and multi-dimensional planning problems efficiently [14,16,21]. These methods are typically applied to determine the optimal location and capacity of storage systems while improving operational indicators such as power losses and voltage profiles.

For example, ref. [16] employed the Whale Optimization Algorithm (WOA) to determine the optimal placement and sizing of BESS in distribution networks. The proposed framework minimizes network power losses under multiple operating conditions and

demonstrates the effectiveness of bio-inspired optimization for storage planning. However, economic considerations associated with BESS investment are not included, and the methodology does not account for uncertainties related to load behavior, equipment outages, or storage system reliability.

Among deterministic approaches for transmission systems, ref. [19] proposed a methodology based on the Developed Harris Hawks Optimization (DHHO) algorithm to determine the optimal allocation and sizing of BESS. The optimization framework improves frequency performance by minimizing frequency deviations measured at the BESS interconnection point while coordinating storage operation with the governors of conventional generating units. Although the proposed strategy effectively enhances frequency regulation, it assumes a generic BESS model and does not account for the characteristics of different storage technologies.

Similarly, ref. [20] proposed a planning framework for both transmission and distribution systems based on complex-valued neural networks (CVNNs) and time-domain power flow analysis. The methodology identifies contingency-sensitive buses and optimizes storage placement and capacity while minimizing investment costs and power losses and improving voltage stability. Although contingency scenarios and voltage forecasts are considered, uncertainties associated with load variability, equipment failures, and outage durations are not explicitly modeled. Beyond voltage profile improvement, BESS integration also requires attention to grid strength and converter dynamics. Recent studies have addressed these aspects through short-circuit-ratio constraints in grid-forming storage planning [22] and synchronization stability analysis of interacting grid-following and grid-forming inverters under current limits [23].

Likewise, ref. [21] proposed a simulation-based meta-heuristic framework using Teaching–Learning-Based Optimization (TLBO) to allocate BESS in distribution systems. The objective is to reduce both the cost of electricity purchased from the utility and system power losses over a 24 h operating horizon. Although the approach yields promising results, it is restricted to distribution networks and does not simultaneously determine the optimal storage size or BESS technology.

Although deterministic approaches have demonstrated their effectiveness for improving technical and economic performance, they generally neglect the stochastic nature of power-system operation. In contrast, stochastic approaches explicitly incorporate uncertainties associated with renewable generation, load demand, component failures, and operational contingencies, providing a more realistic representation of actual power-system behavior [13,18,24–29].

A representative example is presented in [13], where a two-stage energy planning framework simultaneously considers renewable energy resources and energy storage systems. The first stage determines the capacity and technology type of energy resources while minimizing investment costs, whereas the second stage evaluates operational performance and potential energy loss costs. Although the methodology incorporates uncertainty and determines both capacity and storage technology, it does not explicitly address the optimal allocation of BESS within the network.

Similarly, ref. [18] proposed a planning methodology for integrating wind energy into bulk power systems through the optimal allocation of BESS. The approach considers Li-ion and VRF battery technologies to minimize the investment, operation, and maintenance costs while accounting for uncertainties in wind generation and load demand. Nevertheless, the optimization framework focuses exclusively on storage allocation and does not determine the optimal storage capacity.

Another stochastic planning strategy is presented in [28]. Authors use BESS flexibility is used to support voltage regulation in distribution networks. The optimization model

minimizes energy costs, storage operating costs, and penalties associated with transformer overloading and voltage limit violations while considering uncertainties in load demand and photovoltaic generation. Despite its comprehensive treatment of uncertainty, the methodology does not address storage sizing or technology selection.

Additionally, ref. [30] developed a reliability assessment framework integrating bi-level sequential Monte Carlo simulation with a detailed BESS degradation model. The methodology evaluates the influence of storage degradation on system reliability while accounting for the stochastic behavior of transmission system components. However, the framework is primarily focused on reliability assessment rather than optimal storage planning.

Stochastic methodologies typically incorporate uncertainties associated with renewable generation, load demand, or component degradation but frequently address only specific aspects of the planning problem. Further works could examine the joint treatment of BESS allocation sizing, storage technology selection, and transmission system reliability within a unified planning framework. Furthermore, the influence of substation configurations, component failure rates, and storage system reliability characteristics on optimal BESS deployment decisions warrants further investigation. These limitations highlight the need for a comprehensive reliability-oriented planning methodology capable of identifying BESS configurations that enhance transmission system adequacy under uncertain operating conditions.

1.3. Contributions

Table 1 compares representative BESS studies with the proposed methodology (PM) across seven criteria. These include BESS location and sizing, consideration of two or more storage technologies, reliability-oriented planning, failure modeling of multiple component types, daily demand profiles, and cost constraints. The comparison distinguishes the planning decisions addressed by each study from the scope of its reliability modeling and its operating and economic assumptions.

Table 1. Comparison of representative BESS studies and the proposed methodology.

Aspects Considered	**Selected References**										
	[15]	[16]	[17]	[18]	[19]	[20]	[24]	[25]	[26]	[30]	**PM**
Optimization aspects											
Reliability-oriented planning	×	×	×	×	×	×	×	✓	✓	✓	✓
BESS Sizing	✓	✓	✓	×	✓	✓	✓	✓	✓	✓	✓
BESS Location	✓	✓	✓	✓	✓	✓	✓	✓	✓	×	✓
Multiple storage technologies (two or more)	✓	×	×	✓	×	×	×	×	×	×	✓
Failure modeling of multiple component types	×	×	×	✓	×	×	✓	×	✓	×	✓
Operating assumptions and economic constraints											
Daily demand profile	✓	×	✓	✓	×	✓	✓	✓	×	✓	✓
Cost constraints	×	×	×	✓	×	✓	✓	✓	✓	✓	✓

PM: Proposed ✓: consider by the reference ×: does not consider by the reference.

The selected studies address BESS location and sizing to varying extents. However, the consideration of multiple storage technologies, reliability-oriented planning, and failure modeling of different component types varies across the reviewed studies. Daily demand profiles and cost constraints are also included in different combinations. Although several studies address multiple criteria, none jointly covers all seven aspects summarized in the table.

Building on these contributions, the proposed methodology integrates BESS location, rated active power sizing, and selection between two storage technologies with stochastic reliability models for lines, transformers, substations, and BESS. Daily demand profiles and an investment budget are also considered, while ENS evaluated under generator outage scenarios serves as the optimization objective. The contribution therefore lies in integrating these planning and reliability aspects within a single transmission system framework.

This paper proposes a reliability-oriented planning framework for the optimal allocation, sizing, and technology selection of BESS in transmission systems. In this work, sizing refers exclusively to the rated active power capacity (MW) of each BESS. Energy capacity (MWh) is not optimized or explicitly modeled in the reliability assessment. By integrating reliability assessment with a Mixed Gray Wolf Optimizer (MGWO), the proposed methodology identifies storage configurations that enhance system adequacy under uncertain operating conditions. The main contributions of this work are summarized as follows:

- A comprehensive planning methodology is developed that simultaneously determines the optimal allocation, sizing, and technology selection of BESS in transmission systems by using an MGWO-based hierarchical strategy.
- The stochastic behavior of transmission networks is explicitly incorporated into the planning formulation through the reliability characteristics of critical system components, including transmission lines, transformers, and substations. This enables the assessment of BESS deployment strategies under realistic operating conditions and contingency scenarios.

1.4. Paper Organization

The remainder of this paper is structured as follows: Section 2 presents the background on reliability-oriented BESS allocation in transmission systems and describes the common aspects considered in the planning formulation. Section 3 introduces the proposed methodology of allocation and sizing of BESS. Section 4 describes the test system and scenarios. Section 5 presents and discusses the results. Finally, Section 6 summarizes the main conclusions, limitations, and future trends.

2. Background on Reliability-Oriented BESS Planning

2.1. Role of BESS in Transmission System Reliability

Modern transmission systems are becoming complex due to the growing variability of electricity demand, the integration of renewable energy resources, aging infrastructure, and the stochastic failure of critical components such as generators, power lines, transformers, and busbars. These factors increase the risk of service interruptions and challenge utilities in maintaining adequate levels of reliability, resilience, and power quality [31].

BESSs have emerged as an effective solution to enhance power system flexibility and reliability. They provide multiple services, including voltage regulation, frequency control, peak-load management, and black-start capability, thereby improving system operation during both normal and contingency conditions [6].

The contribution of a BESS to the reliability of a power system area depends on its location, nominal power, and availability. In this document, sizing refers to the active power capacity, expressed in MW, which constitutes a decision variable together with location and type of technology. The formulation does not optimize energy capacity (MWh) or model changes in state of charge. Therefore, the selected power ratings alone do not determine the duration of supply.

Load variability, extreme weather events, and the aging of transmission assets further increase the likelihood of equipment outages and reduce system operational

flexibility [27,32,33]. These challenges have motivated the development of reliability-oriented planning methodologies that explicitly incorporate probabilistic models of component failures into the BESS planning process [34].

From this perspective, BESS allocation and sizing should be regarded not only as an operational optimization problem but also as a reliability enhancement strategy. Properly deployed storage systems can mitigate the impact of component outages, reduce ENS, and improve the adequacy and resilience of transmission networks.

2.2. Reliability-Oriented Criteria for BESS Allocation and Sizing

The optimal allocation and sizing of BESS require planning methodologies capable of supporting decision-making under uncertain operating conditions. In addition to determining the optimal location and rated power of storage units, these methodologies must evaluate their impact on system performance in the presence of component outages, load variability, and other operational uncertainties. Consequently, probabilistic reliability assessment has become an essential tool for transmission system planning [27].

Figure 1 classifies the criteria commonly adopted for BESS allocation and sizing into four categories: strategic, technical, economic, and reliability-oriented. Strategic criteria prioritize storage deployment according to the geographical distribution or criticality of load centers. Technical criteria aim to improve system operation through voltage regulation, frequency support, congestion relief, and peak-load management, whereas economic criteria seek to minimize investment and operating costs.

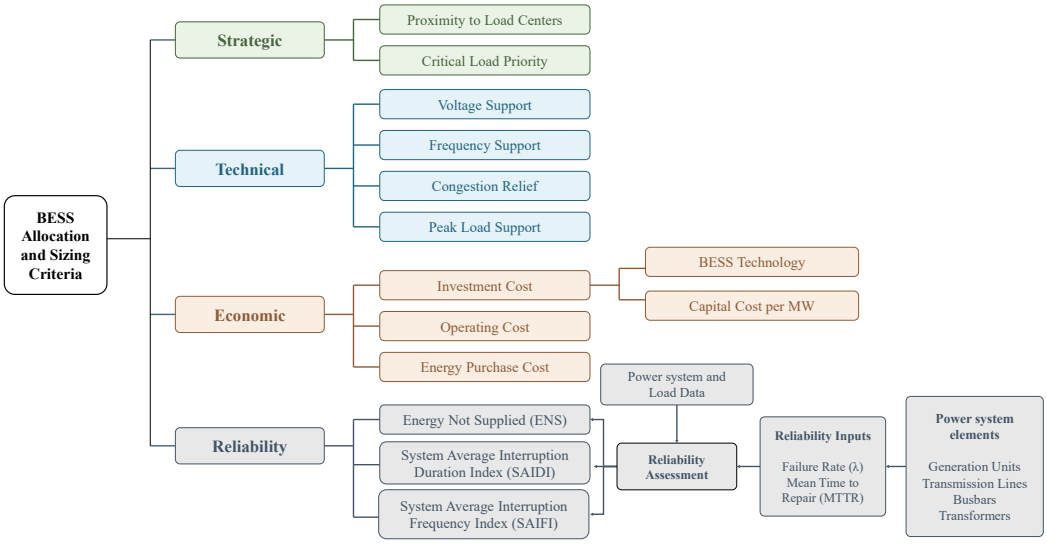


Figure 1. Classification of criteria considered in BESS allocation planning for transmission systems.

Reliability-oriented criteria assess continuity of supply using indicators that describe different consequences of outages. Energy not supplied (ENS) quantifies the energy that is not delivered to loads during the assessment period. The System Average Interruption Duration Index (SAIDI) expresses the cumulative outage time per user, while the System Average Interruption Frequency Index (SAIFI) is the average number of outages per user. These indicators characterize supply reliability by quantifying unserved energy and the duration and frequency of interruptions.

Using a reliability index as an optimization objective does not specify how uncertainty is represented. In many existing studies, indices such as ENS are evaluated under deterministic operating conditions or predefined contingency scenarios. In contrast, reliability-oriented planning explicitly incorporates the stochastic behavior of transmission system components through failure rates, repair rates, and contingency probabilities. In the proposed framework,

component failure and repair rates characterize availability and unavailability, providing data for the reliability assessment used to compare candidate BESS technologies.

Although numerous studies successfully combine technical and economic criteria, only a limited number explicitly integrate probabilistic reliability assessment into the BESS allocation and sizing process. This limitation motivates the methodology proposed in this paper, which incorporates component failure and repair rates into the optimization framework to determine the optimal allocation, sizing, and technology selection of BESS.

2.3. Reliability Impact of Component Failure

When a component in a power system fails, the system goes from a normal operating state to a contingency scenario in which corrective actions are required to prevent violations of operational limits. From a reliability perspective, two-state models represent power system elements characterized by available and unavailable states, as illustrated in Figure 2. Although more detailed multi-state reliability models can represent component degradation or partial operating conditions, the two-state model is sufficiently accurate for power system planning applications because the main objective is to evaluate the impact of component outages on system reliability rather than the physical degradation mechanisms of individual assets. Failure and repair rates describe the transitions between these two states. This representation aligns with the scope of the study, which focuses on evaluating how component outages affect supply continuity, and provides a simplified basis for comparing BESS technologies.

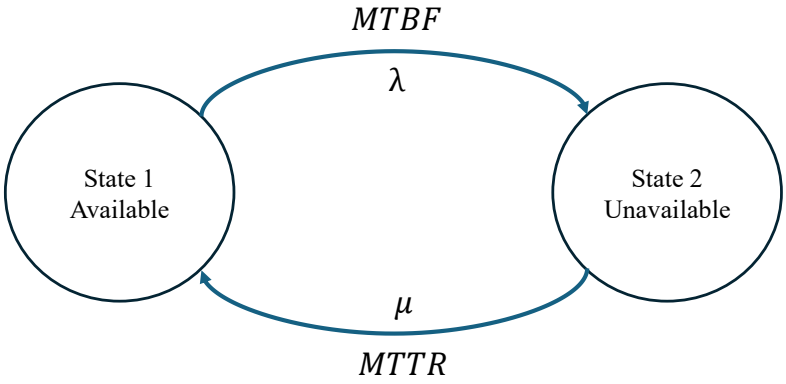


Figure 2. Two-state reliability model of a repairable component.

The failure and repair rates of a repairable component represented by a two-state model are defined in Equations (1) and (2).

$$\lambda = \frac{N_f}{T} = \frac{1}{MTBF}, \tag{1}$$

$$\mu = \frac{N_r}{H_r} = \frac{1}{MTTR}, \tag{2}$$

where N_f is the number of failures recorded during the observation period, T is the cumulative operating time of the component, N_r is the number of completed repairs, and H_r is the cumulative repair time. The steady-state availability and unavailability probabilities P_A and P_U are given by Equations (3) and (4), respectively.

$$P_A = \frac{\mu}{\lambda + \mu} \tag{3}$$

$$P_U = \frac{\lambda}{\lambda + \mu} \tag{4}$$

The failure rate λ and repair rate μ are expressed in failures per hour and repairs per hour, respectively. These parameters influence the frequency and duration of service interruptions and affect reliability indices such as ENS, SAIDI, and SAIFI, making them essential inputs to reliability-oriented BESS planning.

For independent component states, the probability of contingency state k given in Equation (5).

$$Pr_k = \prod_{i \in \mathcal{U}_k} P_{U,i} \prod_{i \in \mathcal{A}_k} (1 - P_{U,i}), \tag{5}$$

where $\mathcal{U}_k$ and $\mathcal{A}_k$ denote unavailable and available components, respectively. For constant demand, the corresponding expected annual ENS is presented in Equation (6).

$$\mathbb{E}[ENS] = 8760 \sum_k Pr_k \sum_j P^{\text{uns}}_{j,k}, \tag{6}$$

where $P^{\text{uns}}_{j,k}$ is the unserved power in MW at load j under state k. For time-varying demand, this expression is evaluated over the demand-profile intervals using their respective durations. Since $P_{U,i} = \lambda_i/(\lambda_i + \mu_i)$, a higher failure rate increases unavailability for a fixed repair rate and may increase ENS when the affected states require load curtailment.

2.4. Reliability-Oriented BESS Planning Problem

Figure 3 illustrates an 11-busbar power system with three generators and five loads. The planning problem considers the installation of two BESS units based on Li-ion and VRF technologies. The objective is to determine the optimal location and capacity of each BESS within the power system to enhance reliability under different operating conditions. In this paper, the sizing of the BESS refers to its nominal power, expressed in MW, and not to its energy capacity, expressed in MWh. The methodology determines BESS locations and rated powers without explicitly optimizing stored energy. A fixed duration of 2 h is assumed solely for investment estimation; energy capacity and chronological state of charge are not explicitly modeled in the reliability assessment.

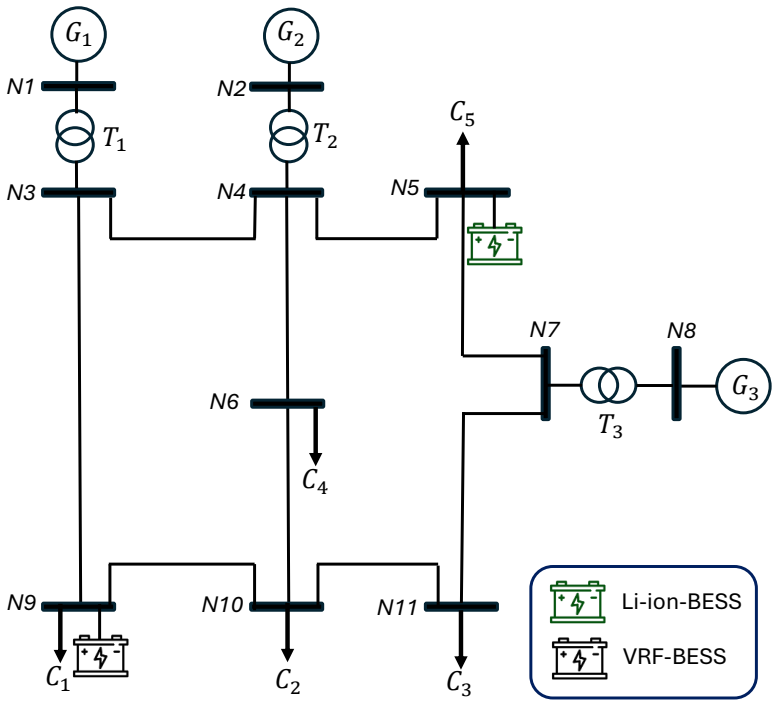


Figure 3. Illustrative transmission system with candidate BESS locations.

Among the reliability indices reported in the literature, ENS is one of the most widely adopted indicators because it quantifies the amount of demand that cannot be served due to component failures, operational constraints, or other contingency events. The optimization process seeks to find the best combination of BESS, including the locations, capacities, and technologies, that minimizes the expected ENS in the whole transmission system.

Equations (7)–(9) describe the objective function for the reliability-oriented planning problem.

$$\min ENS \tag{7}$$

$$ENS = \sum_{j=1}^{N_l} ACIT_j \cdot \left(Pd_j + Ps_j\right) \tag{8}$$

$$ACIT_j = \sum_{k=1}^{N_c} 8760 \cdot Pr_k \cdot frac_{j,k}. \tag{9}$$

where N_l is the number of loads, Pd_j is the active power disconnected at j-th load, and Ps_j represents the active power curtailed in j-th load resulting from system operating constraints. N_c is the number of contingency states, Pr_k is the probability of occurrence of contingency state k, and $frac_{j,k}$ is the fraction of customers at load point j interrupted under that state. Since Pr_k and $\text{frac}_{j,k}$ are dimensionless, the product $8760 \cdot Pr_k \cdot frac_{j,k}$ is expressed in hours per year. Consequently, $ACIT_j$ represents the expected annual customer interruption time associated with load point j.

In this paper, ENS is the optimization criterion used to evaluate and compare BESS configurations. SAIDI and SAIFI are complementary indicators of the reliability framework, presented in Equations (10)–(12). While these indices provide valuable information regarding interruption frequency and duration, ENS offers a more direct measure of the reliability benefits associated with BESS deployment by quantifying the amount of energy that remains unserved during contingency conditions. Therefore, SAIDI and SAIFI complement the conceptual reliability framework by describing the average duration and frequency of supply interruptions per customer, respectively.

$$SAIDI = \frac{\sum_{j=1}^{N_l} ACIT_j \cdot C_j}{\sum_{j=1}^{N_l} C_j} \tag{10}$$

$$SAIFI = \frac{\sum_{j=1}^{N_l} ACIF_j \cdot C_j}{\sum_{j=1}^{N_l} C_j} \tag{11}$$

$$ACIF_j = \sum_{k=1}^{N_c} Fr_k \cdot frac_{j,k} \tag{12}$$

where $ACIF_j$ is the average customer interruption frequency for the j-th load, C_j is the number of customers for the j-th load and Fr_k is the frequency of the occurrence of k-th contingency.

The mathematical formulation of BESS planning introduces the constraints associated with the allocation and sizing of BESS in the power system; these are summarized in Equations (13)–(17). The constraint Equation (13) ensures that the voltage at each node is within the limits. Similarly, constraint Equation (14) ensures that the magnitude of the power flow through each branch j does not exceed its maximum allowable value P_{max_j}, regardless of the flow direction.

$$V_{min} \leq V_j \leq V_{max} \quad \forall \; j = 1, \cdots, N_n \tag{13}$$

$$0 \leq P_j \leq P_{max_j} \quad \forall \; j = 1, \cdots, N_b \tag{14}$$

Equation (15) expresses the active power balance at each bus, accounting for generation, demand, and power exchanges with connected branches. The feasibility of each MGWO candidate solution is checked through power flow calculations under the operating conditions considered.

$$P_{G,i} - P_{D,i} = \sum_{k \in \Omega_i} P_{l,ik} \tag{15}$$

Equations (16) and (17) impose the power capacity limits for BESS types 1 and 2, respectively. The next section presents the proposed optimization framework for BESS allocation and sizing.

$$0 \leq P_{BS1,k} \leq PBS_{1max} \quad \forall \; k = 1, \cdots, NBS_1 \tag{16}$$

$$0 \leq P_{BS1,h} \leq PBS_{2max} \quad \forall \; h = 1, \cdots, NBS_2 \tag{17}$$

where NBS_1 and NBS_2 are the numbers of BESS considered are of the type 1 and 2, respectively. The variables $P_{BS1,k}$ and $P_{BS2,h}$ denote their rated active power capacities.

3. Optimal Strategy to Allocate and Size BESS Considering a Reliability-Oriented Approach

The proposed methodology seeks to determine the optimal allocation and sizing of two BESS technologies, Li-ion and VRF, in a transmission system. Figure 4 illustrates the proposed methodology, which comprises four stages. The first stage establishes stochastic models for the main components of the transmission system, including transmission lines, transformers, and substations. The second stage defines the initial technical and economic parameters of the BESS; additionally, the transmission system is modeled according to the characteristics of its components and the load demand profiles. The third stage presents the Mixed Gray Wolf Optimizer (MGWO) technique employed to solve the BESS allocation and sizing problem. Finally, the fourth stage describes the procedure used to evaluate the ENS for the feasible solutions obtained by the MGWO algorithm. In the following subsections, each stage of the methodology is described in detail.

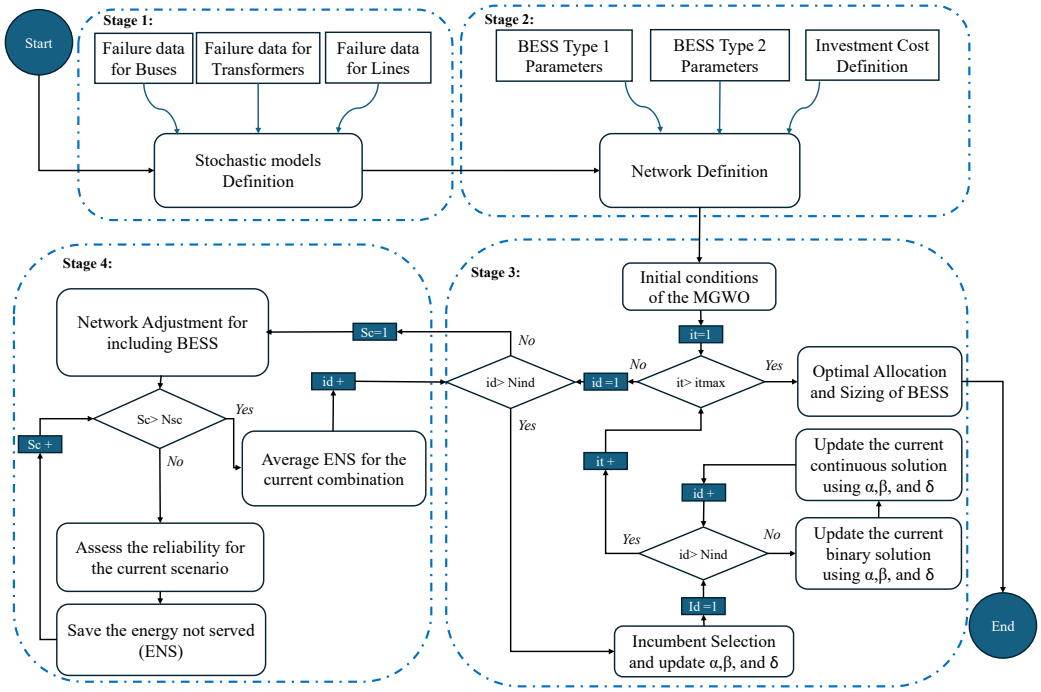


Figure 4. Flowchart of the methodology for allocating and sizing BESS.

3.1. Stage 1: Definition of Stochastic Models for Network Components

Stage 1 defines the stochastic models for system components such as transmission lines, transformers, and busbars, which are represented statistically through their failure rate λ and mean time to repair $MTTR$. Accordingly, each element is characterized by its own failure data. Table 2 presents the parameters considered for each transmission line and transformer of the analyzed system. These failure and repair parameters constitute the input data used by the reliability-assessment module to generate the component states and their associated probabilities and frequencies.

Table 2. Reliability parameters for transmission lines and transformers.

Lines	Failure Rate	MTTR [h]	Transformers	Failure Rate	MTTR [h]
$Line_1$	λ_{L1}	$MTTR_{L1}$	$Transformer_1$	λ_{T1}	$MTTR_{T1}$
$Line_2$	λ_{L2}	$MTTR_{L2}$	$Transformer_2$	λ_{T2}	$MTTR_{T2}$
...	...	...	...	...	....
$Line_M$	λ_{LM}	$MTTR_{LM}$	$Transformer_K$	λ_{TK}	$MTTR_{TK}$

The values of λ and MTTR are specified according to the busbar arrangement. Table 3 lists typical configurations used in transmission systems, each characterized by its own failure rate and mean time to repair.

Table 3. Typical failure data for busbar configurations.

Type of Configuration	Failure Rate	MTTR [h]
Single Busbar	λ_{SB}	$MTTR_{SB}$
Main and transfer	λ_{MT}	$MTTR_{MT}$
Ring Busbar	λ_{RB}	$MTTR_{RB}$
Breaker-and-a-half	λ_{BH}	$MTTR_{BH}$

3.2. Stage 2: BESS Initialization and Network Considerations

Stage 2 involves two main processes. The first is the definition of stochastic models for the considered BESS technologies, and the second is the development of the network model. Both processes are described in detail in the following sections.

3.2.1. Stochastic Reliability Model for BESS

Each BESS technology is represented by a two-state reliability model, as described in Section 2.3, which is a conventional approach to representing the failure behavior of a component [35]. Accordingly, each BESS technology is characterized by its own stochastic reliability model, defined by parameters such as the probability of occurrence of each state, the failure duration, and the total time spent in each state. In the available state, the BESS can absorb or inject active power; in the unavailable state, it is out of service due to failure or maintenance. In this way, the expected available active power capacity of the BESS, denoted by P_{BESS}, can be modeled as a function of the forced outage expectancy (FOE), according to Equation (18).

$$P_{BESS,i} = P_{nom} \cdot \left(1 - \frac{FOE}{8760}\right) \tag{18}$$

where P_{nom} is the nominal active power capacity of the BESS technology to be installed, and FOE is the expected number of hours during which the device is unavailable over a one-year period.

The proposed methodology optimizes P_{nom} in MW as the continuous BESS sizing variable. The BESS units are implemented in DIgSILENT PowerFactory using a voltage-based

control model, with minimum and maximum SOC settings of 10% and 90%, respectively. However, the reliability assessment does not explicitly propagate SOC between successive operating conditions or model charging and discharging durations and efficiencies through a chronological energy balance. Therefore, these device-level settings do not establish an energy-limited contribution to the calculated ENS. The fixed duration of 2 h is used solely for investment estimation, and sufficient stored energy is assumed during each evaluated contingency. Consequently, the obtained results represent BESS power capacity requirements rather than a complete storage system sizing in both MW and MWh.

For the adopted two-state reliability model, the BESS availability and unavailability probabilities are determined from its failure and repair rates. The repair rate is obtained from the mean time to repair as shown in Equation (2).

Since the failure rate data are reported in failures per year, the annual failure rate λ_y is converted to an hourly rate according to Equation (19).

$$\lambda_h = \frac{\lambda_y}{8760}. \tag{19}$$

Assuming constant failure and repair rates, the steady-state availability and unavailability probabilities are calculated by Equation (20), respectively.

$$P_A = \frac{\mu}{\lambda_h + \mu}, \qquad P_U = \frac{\lambda_h}{\lambda_h + \mu}. \tag{20}$$

The forced outage expectancy represents the expected number of hours during which the BESS is unavailable over a one-year period and is obtained according to Equation (21).

$$FOE = 8760 \cdot P_U = 8760 \cdot \left(\frac{\lambda_h}{\lambda_h + \mu} \right). \tag{21}$$

The two-state formulation represents the BESS as an aggregated repairable component and captures its transition between complete availability and complete unavailability. It does not explicitly distinguish between failures of internal subsystems or partial-capacity operating states. These limitations and their corresponding future extensions are discussed in Section 6.2.

3.2.2. Generation Dispatch and Demand Profiles

The network model incorporates hourly demand variation and generation dispatch. Historical load data covering one year is used to construct representative weekday, Saturday, and Sunday profiles. Each load is represented by three demand curves: one for a typical weekday, one for a typical Saturday, and one for a typical Sunday. The hourly active and reactive power values for a typical day are obtained by using Equations (22)–(25).

$$P_{t_{j_i}} = \{P_{1_t}, P_{2_t}, P_{3_t}, \ldots, P_{Nd_t}\} \quad \forall \quad j \in \beta = \{Weekday, Saturday, Sunday\} \tag{22}$$

$$Pact_{t_{j_k}} = \frac{1}{Nd} \sum_{k=1}^{N_d} P_{k_t} \tag{23}$$

$$Q_{t_{j_i}} = \{Q_{1_t}, Q_{2_t}, Q_{3_t}, \ldots, Q_{Nd_t}\} \quad \forall \quad j \in \beta = \{Weekday, Saturday, Sunday\} \tag{24}$$

$$Qact_{t_j} = \frac{1}{Nd} \sum_{k=1}^{N_d} Q_{k_t} \tag{25}$$

where $P_{t_{j_i}}$ and $Q_{t_{j_i}}$ are the sets of historical active and reactive power data measured for the i-th load in the t-th period for the j-th typical day, Nd is the number of samples for the t-th period in the j-th typical day and $Pact_{t_{j_i}}$ and $Qact_{t_{j_i}}$ are the average active and reactive

powers for the i-th load in the t-th period for the j-th typical day, respectively. Once the values for each hour are obtained, the typical demand curve can be drawn.

The available measurements were classified according to the type of day into three categories: weekdays, Saturdays, and Sundays. Subsequently, for each category and for each time of day, the corresponding historical observations were grouped and averaged according to Equations (22)–(25). This procedure produces three representative 24 h profiles that capture the typical intraday variation in system demand. These typical profiles were subsequently used to represent the behavior of demand during the annual reliability evaluation.

Generation dispatch is then determined using an optimal power flow. The resulting generator outputs define the dispatch profiles for the assessment period. In Equation (26), Pg_{tj} denotes the vector of active power outputs of the N_g generators at hour t for day type j.

$$Pg_{t_j} = \left\{Pg_{1_t}, Pg_{2_t}, Pg_{3_t}, \ldots, Pg_{Ng_t}\right\} \quad \forall \quad j \in \beta = \{Weekday, Saturday, Sunday\} \tag{26}$$

The dispatch is obtained through an AC optimal power flow (OPF) for each hour of the representative weekday, Saturday, and Sunday. The objective of the OPF is to minimize the total active power losses in the transmission network. The calculation is subject to the nodal active- and reactive power balance equations, the minimum and maximum active- and reactive power limits of the generation units, the allowable voltage-magnitude limits at each bus, and the maximum loading limits of the transmission branches. A reference angle is also assigned to the slack bus to provide a unique power flow solution.

The hourly active power outputs obtained from the OPF are used to construct the generation dispatch curves defined in Equation (26). This calculation represents the base operating condition of the system and is performed before the MGWO determines the location, technology, and rated power of the candidate BESS units. Consequently, BESS charging and discharging are not included in the OPF, and neither energy capacity nor state-of-charge constraints are considered at this stage.

3.3. Stage 3: Mixed Gray Wolf Optimization (MGWO)

Stage 3 incorporates the optimization algorithm responsible for determining the optimal BESS deployment strategy. The planning problem involves both discrete and continuous decision variables. The discrete variables determine the installation status and technology of each BESS, whereas the continuous variables determine their rated active power capacities P_{nom} in MW, as defined in Section 3.2.1. Owing to this mixed-integer search space, MGWO is adopted to simultaneously optimize the allocation, power capacity sizing, and technology selection of the storage systems.

MGWO is selected because it can solve highly nonlinear optimization problems with mixed decision variables efficiently while maintaining a suitable balance between global exploration and local exploitation. These characteristics make the algorithm particularly appropriate for reliability-oriented BESS planning, where the objective function depends on both network operating conditions and the stochastic behavior of transmission system components.

The optimization strategy is based on the Gray Wolf Optimizer (GWO), a population-based meta-heuristic inspired by the social hierarchy and cooperative hunting behavior of gray wolves [36]. The population is organized into four hierarchical levels. The three best candidate solutions are identified as the α, β, and δ wolves, which guide the search process, while the remaining solutions are classified as ω wolves. During each iteration, the population updates its positions by following the leading wolves, allowing the algorithm to converge progressively toward the optimal solution.

The leaders guide the movement of the ω population toward more promising regions of the search space, thereby promoting an effective balance between exploration and exploitation in a highly nonlinear optimization environment.

The representation of a wolf, or candidate solution, for the BESS allocation and sizing problem is depicted in Figure 5. Each wolf corresponds to a specific combination of two BESS technologies: BESS type 1 (Li-ion) and BESS type 2 (VRF), which can be installed at different busbar of the case study. Accordingly, each busbar is modeled using a binary decision variable that indicates the installation status of a BESS and a continuous decision variable that represents its rated active power capacity. A value of 1 denotes that a BESS is installed at the corresponding node, whereas a value of 0 indicates that no BESS is connected.

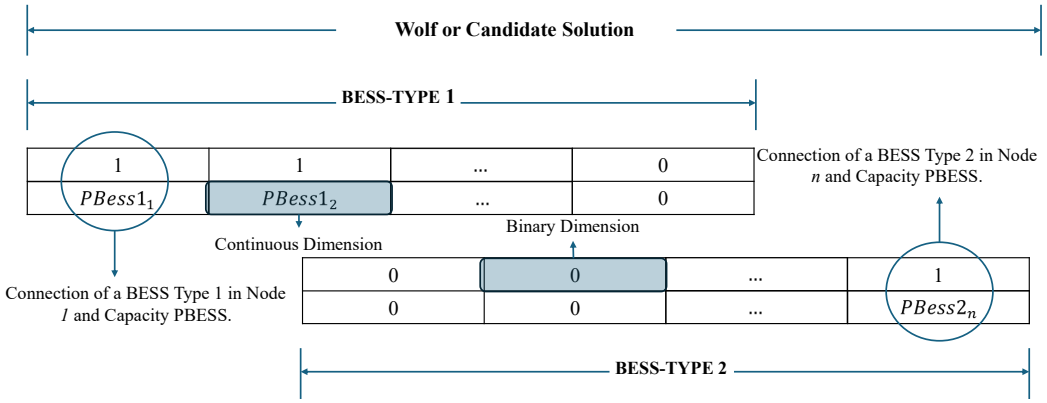


Figure 5. Candidate solution representation for MGWO.

When a BESS is installed, its active power rating is assigned within the minimum and maximum power limits of the selected technology. The MGWO identifies the three best solutions, denoted as α, β, and δ, which yield the lowest fitness function values. The remaining candidate solutions, denoted as ω, are subsequently updated at each iteration to search for improved fitness values. Whenever a superior solution emerges, the leader solutions α, β, and δ are updated accordingly to preserve the hierarchical structure of the algorithm.

The position-update mechanism applied at each iteration depends on the type of decision variable. Each candidate solution contains a binary vector X_{it}, which determines the installation status of the BESS units, and a continuous vector PX_{it}, which determines their rated active power capacities. The binary and continuous components must therefore be updated using different operators.

Let $\mathcal{L} = [\alpha, \beta, \delta]$ denote the three leading solutions. For each omega wolf and dimension d, the algorithm calculates three leader-guided candidate positions associated with the α, β, and δ wolves. For the binary variables, these positions are denoted by X_1^d, X_2^d, and X_3^d, whereas PX_1^d, PX_2^d, and PX_3^d denote the corresponding positions for the continuous variables. The binary update follows the procedures presented in [37,38], while the continuous update is based on the original GWO formulation described in [36].

The coefficients required for the position-update process are calculated using Equations (27)–(31). This procedure is performed for every dimension of each candidate solution and is repeated for all wolves throughout the optimization process. Algorithm 1 summarizes the mixed-variable position-update procedure.

$$\mathcal{L} = [\alpha, \beta, \delta], \tag{27}$$

$$A_{\mathcal{L}_j}^d = 2ar_{1,j}^d - a, \qquad r_{1,j}^d \sim U(0,1), \qquad j = 1,2,3, \tag{28}$$

$$C_{\mathcal{L}_j}^d = 2r_{2,j}^d, \qquad r_{2,j}^d \sim U(0,1), \qquad j = 1,2,3, \tag{29}$$

$$D_{\mathcal{L}_j}^d = \left| C_{\mathcal{L}_j}^d X_{\mathcal{L}_j,it}^d - X_{it}^d \right|, \qquad j = 1,2,3, \tag{30}$$

$$Cstep^{d}_{\mathcal{L}_j} = \frac{1}{1+\exp\left[-10\left(A^{d}_{\mathcal{L}_j} D^{d}_{\mathcal{L}_j} - 0.5\right)\right]}, \qquad j = 1,2,3. \tag{31}$$

Algorithm 1: Mixed-variable position update for an omega wolf.

Data: Maximum number of iterations $it_{\max}$; current iteration it; current wolf (X_{it}, PX_{it}); leader wolves $(X^{\alpha}_{it}, PX^{\alpha}_{it})$, $(X^{\beta}_{it}, PX^{\beta}_{it})$, and $(X^{\delta}_{it}, PX^{\delta}_{it})$; number of dimensions N_d

Result: Updated wolf (X_{it+1}, PX_{it+1})

$\mathcal{L} \leftarrow [\alpha, \beta, \delta]$;
$a \leftarrow 2 - 2it/it_{\max}$;
for $d \leftarrow 1$ **to** N_d **do**
  for $j \leftarrow 1$ **to** 3 **do**
    Generate $r^{d}_{1,j}, r^{d}_{2,j}, r^{d}_{3,j} \sim U(0,1)$;
    Compute $A^{d}_{\mathcal{L}_j}$, $C^{d}_{\mathcal{L}_j}$, $D^{d}_{\mathcal{L}_j}$, and $Cstep^{d}_{\mathcal{L}_j}$ using (28)–(31);
    if $Cstep^{d}_{\mathcal{L}_j} \geq r^{d}_{3,j}$ **then**
      $Bstep^{d}_{\mathcal{L}_j} \leftarrow 1$;
    else
      $Bstep^{d}_{\mathcal{L}_j} \leftarrow 0$;
    if $X^{d}_{\mathcal{L}_j,it} + Bstep^{d}_{\mathcal{L}_j} \geq 1$ **then**
      $X^{d}_{j} \leftarrow 1$;
    else
      $X^{d}_{j} \leftarrow 0$;
  Generate $r^{d}_{4} \sim U(0,1)$;
  if $r^{d}_{4} \leq 1/3$ **then**
    $X^{d}_{it+1} \leftarrow X^{d}_{1}$;
  else
    if $r^{d}_{4} \leq 2/3$ **then**
      $X^{d}_{it+1} \leftarrow X^{d}_{2}$;
    else
      $X^{d}_{it+1} \leftarrow X^{d}_{3}$;
  if $X^{d}_{it+1} = 0$ **then**
    $PX^{d}_{it+1} \leftarrow 0$;
  else
    for $j \leftarrow 1$ **to** 3 **do**
      $D^{d}_{\mathcal{L}_j,P} \leftarrow \left|C^{d}_{\mathcal{L}_j} PX^{d}_{\mathcal{L}_j,it} - PX^{d}_{it}\right|$;
      $PX^{d}_{j} \leftarrow PX^{d}_{\mathcal{L}_j,it} - A^{d}_{\mathcal{L}_j} D^{d}_{\mathcal{L}_j,P}$;
    $PX^{d}_{it+1} \leftarrow \left(PX^{d}_{1} + PX^{d}_{2} + PX^{d}_{3}\right)/3$;
    Apply the minimum and maximum power capacity limits;
return (X_{it+1}, PX_{it+1});

For each binary dimension, three candidate values are generated from the α, β, and δ wolves and one of them is selected through a crossover operator with equal probability. For each continuous dimension, the three leader-guided positions are averaged following the original GWO update rule. If the binary variable associated with a given node is zero, its corresponding continuous power capacity is also set to zero. Otherwise, the updated capacity is restricted to the minimum and maximum limits of the selected BESS technology.

This update procedure is applied to every omega wolf at each iteration, after which the fitness values are recalculated and the α, β, and δ solutions are updated.

3.4. Stage 4: Reliability Evaluation

This stage defines an ENS-based fitness function to evaluate candidate BESS configurations. The formulation is modified with respect to Equation (8). In the proposed approach, the ENS-based fitness function is evaluated over a set Γ containing N_g single-generator-outage scenarios. In each scenario $\gamma_i \in \Gamma$, one generator is assumed to be unavailable, and the ENS is calculated by applying the annual reliability assessment to the remaining system components. The fitness function is defined in Equation (32).

$$\min F(\mathbf{x}) = \frac{1}{N_g} \sum_{\gamma_i \in \Gamma} ENS_{\gamma_i}(\mathbf{x}), \tag{32}$$

where $\mathbf{x}$ represents the BESS allocation and sizing decision, $ENS_{\gamma_i}(\mathbf{x})$ is the annual ENS obtained under the i-th generator-outage scenario, and N_g is the total number of evaluated scenarios.

An equal weight of $1/N_g$ is assigned to every scenario because the objective is to evaluate the average robustness of each candidate BESS solution across the complete set of $N-1$ generator-outage conditions, rather than to estimate the probability-weighted ENS associated with generator failures. This prevents the optimization from prioritizing a particular generator-outage scenario. Since N_g is constant, minimizing the arithmetic mean is equivalent to minimizing the sum of the ENS values, while providing a normalized fitness measure that facilitates the comparison of candidate solutions.

The reliability evaluation of each candidate BESS configuration is performed using DIgSILENT PowerFactory, whereas the MGWO optimization process and the exchange of input and output data are managed through Python 3.10. For each candidate solution, Python updates the location, technology, and rated power of the BESS units in the network model and executes the reliability-assessment module.

The failure and repair parameters assigned to the transmission lines, transformers, busbars, and BESS units are used to define their stochastic reliability models. Based on these models and the considered load conditions, the system-state generation procedure identifies the relevant contingency states and determines their probabilities Pr_k and occurrence frequencies Fr_k. A failure-effect analysis is then performed for each state to identify the interrupted load and the fraction of customers affected at each load point.

The mathematical model employed to determine the optimal allocation and sizing of BESS considers not only the constraints described in Section 2.4 but also the additional constraints defined in Equations (33) and (34). These supplementary constraints ensure that the algorithm avoids infeasible solutions, such as configurations exceeding the maximum allowable investment cost or scenarios in which two different types of BESS are simultaneously installed at the same bus.

$$\sum_{k=1}^{NBS_1} W_1 \cdot PBS_{1_k} + \sum_{h=1}^{NBS_2} W_2 \cdot PBS_{2_h} \leq Cost_{max} \tag{33}$$

$$BS_{1_i} + BS_{2_i} \leq 1 \;\; \forall \;\; i \;\; \in Nodes = 1, 2, \cdots, N_n \tag{34}$$

Here, W_1 and W_2 denote the initial capital costs per MW of installed rated power for Li-ion and VRF BESS, respectively. They incorporate both power-related and energy capacity-related capital components, assuming a fixed duration of 2 h solely for cost estimation. These coefficients represent equipment and installation investment, rather than electricity prices or costs per MWh delivered. Energy capacity is not independently optimized, and charging-energy, operation, maintenance, and replacement costs are excluded.

The fitness function is evaluated through a reliability analysis based on hourly power flow simulations over a period of one year, as illustrated in Figure 6, where N_{CS} denotes the number of contingency states and N_{LS} represents the number of load states. This analysis generates a comprehensive set of system states derived from the adopted failure and load models, from which the relevant operating conditions are identified.

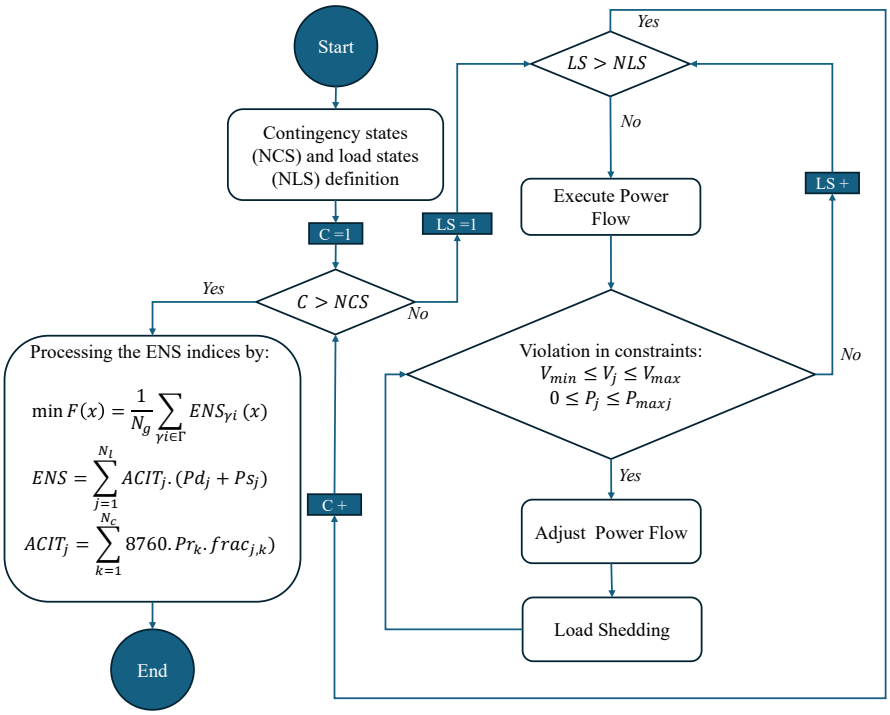


Figure 6. Strategy for evaluating ENS within the proposed methodology.

Whenever the constraints defined in Equations (13) and (14) are violated, a load-shedding procedure is implemented until the violations are resolved. The amount of curtailed load directly impacts the fitness function through Equation (32), since the system must reduce demand to restore admissible operating conditions, thereby increasing the resulting ENS value.

4. Case Study

The proposed methodology is evaluated through three complementary case studies. The first examines BESS planning without an investment limit. The second investigates the influence of investment limits, and the third assesses the consistency of the optimization results across independent runs.

4.1. Test System

The methodology is evaluated using the modified IEEE 39-bus New England test system, shown in Figure 7 [39]. This network comprises 10 generators, 46 transmission lines, and 19 three-phase loads, and operates at a nominal voltage level of 350 kV. Its main characteristics include balanced loads and an equivalent external network connected at bus 1.

The modifications introduced for this study include: (1) three representative 24 h load profiles based on Colombian demand values for Monday–Friday, Saturday, and Sunday; (2) an optimal dispatch strategy to determine the active power outputs of the generators; and (3) breaker-and-a-half configurations at all substations. The system is implemented

in DIgSILENT PowerFactory, where the three demand profiles are extrapolated over a complete one-year reliability assessment horizon, as described in Section 3.2.2.

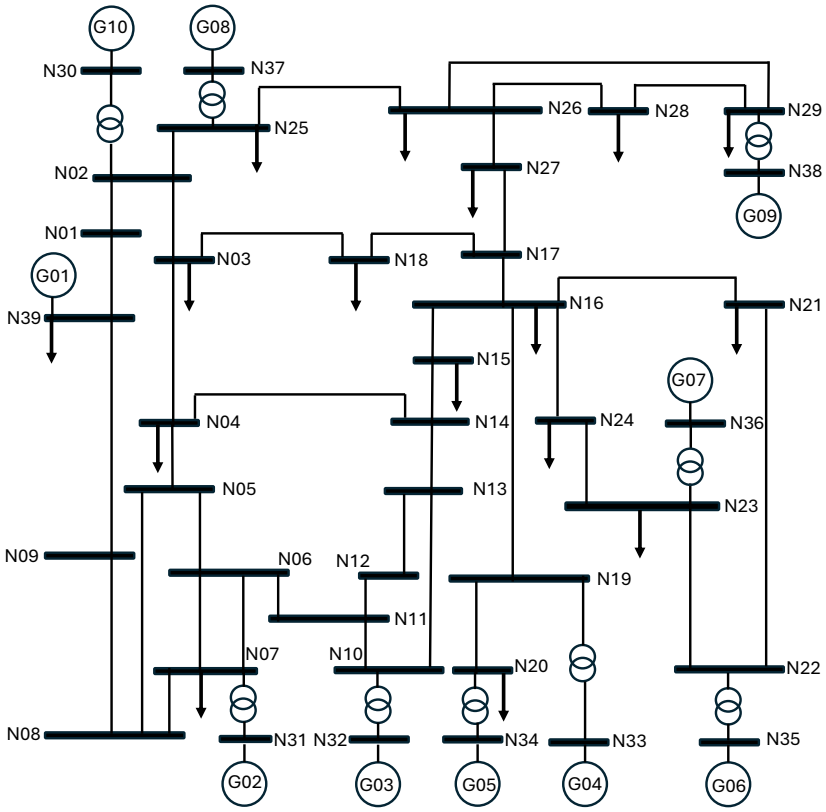


Figure 7. Modified IEEE 39-bus New England test system.

4.2. Case 1: Unrestricted Scenario

In this case, the proposed methodology is configured to determine the incumbent solution without cost restrictions. Therefore, the cost constraint (33) is omitted in mathematical formulation. Table 4 summarizes the failure rates and MTTR values used as input parameters for transmission lines, transformers, and busbar configurations. These parameters were selected based on representative values commonly reported in the specialized literature [40,41].

Table 4. Reliability data for components of the IEEE 39-bus test system.

Component	Failure Rate [1/a]	MTTR [h]
Lines	0.02–0.03	1–6
Transformers	0.5–3.0	0.5–4
Busbars (Breaker and Half Arrangement)	0.05	2

In the absence of component-specific historical failure records for the IEEE 39-bus test system, the ranges presented in Table 4 were used to generate a heterogeneous reliability dataset. For each transmission line and transformer, one failure rate value and one MTTR value were independently sampled from a uniform distribution within the corresponding range. For buses, the fixed values reported in the table were directly assigned. This sampling procedure was performed only once during model initialization, and the resulting component-specific parameters were kept unchanged throughout all reliability evaluations, generator-outage scenarios, MGWO iterations, and planning cases. These parameters were

subsequently used to calculate the repair rates, component unavailability, and contingency probabilities required by the reliability model.

The BESS reliability parameters are common to all case studies: annual unavailability is assumed to be 5% for Li-ion (438 h/year) and approximately 6.5% for VRF (569 h/year). The Li-ion assumption is informed by ISO New England's 5% EFORd planning benchmark, although EFORd differs from annual unavailability [42]. The VRF value is a scenario assumption; the literature identifies relevant component failure mechanisms but does not establish this percentage [43]. These parameters determine the expected available power defined in Section 3.2.1 and do not imply an inherent reliability ranking between technologies.

Furthermore, the initial parameters of the MGWO algorithm for the proposed BESS allocation and sizing methodology are summarized in Table 5. The population size and maximum number of iterations were selected through trial-and-error tuning based on repeated simulations.

Table 5. MGWO parameters and BESS power limits for Case 1.

Description	Value
Number of wolves	10
Maximum number of iterations	160
Maximum capacity for BESS 1 [MW]	80
Maximum capacity for BESS 2 [MW]	50

4.3. Case 2: Restricted Scenario

In this case, the mathematical formulation of the proposed methodology incorporates the cost constraint defined in Equation (33). This constraint limits the total investment in BESS deployment, including technology selection and power capacity sizing. Accordingly, any solution exceeding this predefined investment limit is considered infeasible.

Investment budgets from 100 to 750 MUSD are evaluated in increments of 50 MUSD. An independent optimization is performed for each budget. This procedure aims to identify the investment thresholds at which the methodology yields the lowest fitness function values. The investment coefficients are informed by the component-level cost projections for 2025 in [44]. Assuming a duration of 2 h, these yield approximately 0.876 MUSD/MW for Li-ion and 1.452 MUSD/MW for VRF. The adopted values of 0.80 and 1.30 MUSD/MW are simplified planning assumptions, approximately 9–10% below these estimates, with a similar relative cost ratio. Only initial investment is considered; operation, maintenance, and replacement costs are excluded.

The failure rate and MTTR data employed are identical to those reported in Table 4. The parameters used to initialize the proposed methodology are summarized in Table 6.

Table 6. Planning and optimization parameters for Case 2.

Description	Value
Number of wolves	10
Maximum number of iterations	160
Maximum investment cost [MUSD]	100 to 750
Cost of investment per MW of BESS 1 [MUSD/MW]	0.80
Cost of investment per MW of the BESS 2 [MUSD/MW]	1.30
Maximum capacity for BESS 1 [MW]	80
Maximum capacity for BESS 2 [MW]	50

4.4. Case 3: Performance of the Best Solution

This case evaluates the consistency of the proposed methodology and the MGWO algorithm under an investment budget constraint. To this end, the scenario selected as a representative compromise between investment cost and reliability performance is considered. Ten independent optimization runs are performed using the same input data and algorithm parameters specified in Tables 4 and 6.

Additionally, the convergence behavior of the MGWO algorithm is assessed for the selected scenario by analyzing the evolution of the fitness function over the maximum number of iterations.

5. Results and Discussion

This section presents the results of the performance of the proposed BESS allocation and sizing strategy, as well as the respective discussion. The analysis considered different cases established in Tables 4–6. The results for the cases described in Section 4 are presented below.

5.1. Unrestricted Scenario Analysis

Figure 8 presents the convergence behavior of the fitness function for the proposed BESS allocation and sizing strategy.

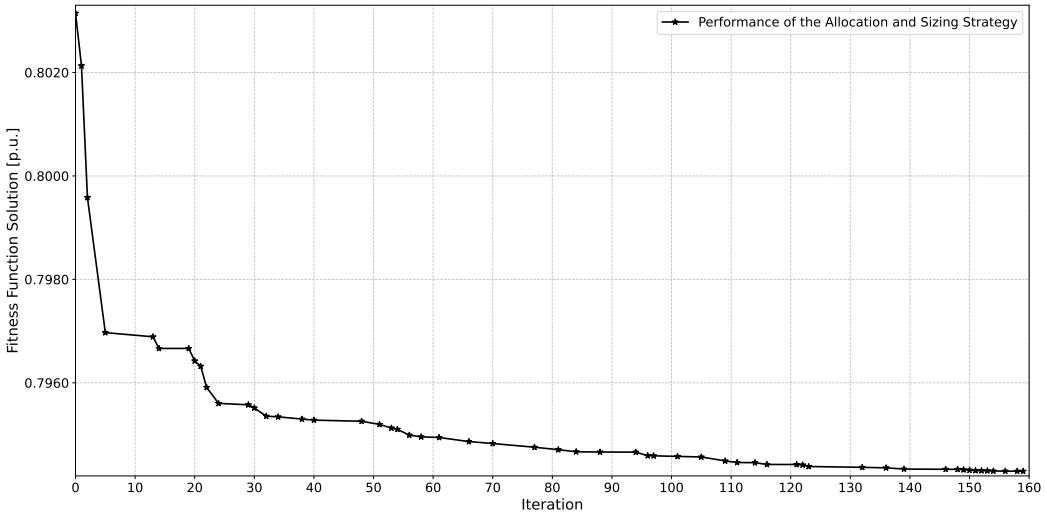


Figure 8. Fitness convergence in the unrestricted scenario.

To facilitate interpretation, the fitness values are normalized with respect to the ENS obtained in the reference case without BESS, which is 1,014,512. 67 MWh/year.

The fitness value starts at 0.8031 p.u. and decreases sharply during the first 20 iterations, reaching approximately 0.7965 p.u. This rapid initial decrease is consistent with the exploration phase, during which candidate solutions are updated across the search space.

After iteration 25, the fitness value decreases more gradually and stabilizes near 0.7945 p.u. around iteration 140. This behavior indicates that the algorithm converged to a stable solution within the defined iteration limit, and the optimization process successfully balanced exploration and exploitation.

Table 7 summarizes the installed capacity for each technology type in the test system. The total installed BESS capacity is approximately 868 MW, of which 57.5% is provided by BESS1 and 42.5% by BESS2. The corresponding fitness value is 805,817. 95 MWh/year. Buses 7 and 8 hold the largest capacities, at 77.18 MW and 76.95 MW respectively. The two smallest installed capacities are 1.34 MW at bus 36 and 1.19 MW at bus 21. Notably, considers not only the constraints described in Section 2.4 but also the additional constraints

indicating that both technologies are distributed selectively rather than installed uniformly across the system. The optimized BESS configuration reduces ENS and improves customer-oriented reliability indices, achieving reductions of 27.59% in SAIDI and 27.21% in SAIFI relative to the reference case.

Table 7. BESS allocation and rated power in the unrestricted solution.

BUS	BESS 1 Rated Power [MW]	BESS 2 Rated Power [MW]
1	1.54	0.0
2	16.22	0.0
4	49.24	0.0
5	0.0	14.38
6	0.0	9.97
7	77.18	0.0
8	76.95	0.0
9	0.0	18.64
10	0.0	18.01
11	0.0	14.98
12	0.0	4.05
13	9.82	0.0
14	56.71	0.0
15	0.0	2.15
17	32.78	0.0
18	0.0	30.11
19	11.64	0.0
20	2.82	0.0
21	1.19	0.0
22	33.54	0.0
23	0.0	13.51
26	35.99	0.0
27	0.0	49.05
28	0.0	37.59
29	0.0	49.03
30	32.66	0.0
31	56.81	0.0
32	0.0	30.06
33	0.0	3.19
34	0.0	6.94
35	0.0	6.26
36	1.34	0.0
37	0.0	13.80
38	0.0	46.95
39	2.93	0.0
Total BESS Power [MW]	499.36	368.67
SAIDI Reduction [%]	27.59	
SAIFI Reduction [%]	27.21	
Fitness Function [MWh/year]	805,817.95	

Figure 9 shows the BESS locations in the IEEE 39-bus system. Gray buses indicate BESS1 installations, whereas blue buses indicate BESS2 installations. The blue buses, which indicate BESS2 installations, are located mainly near generation buses and load points. To quantify the effect of the proposed solution on the network, the loading of lines and transformers was compared before and after installing the BESS. The average loading of the

transmission lines decreased from 39.98% to 38.72%, a relative reduction of 3.15%, and the average loading of the transformers decreased from 59.17% to 57.83%, a relative reduction of 2.26%. These results indicate that BESS deployment reduces both ENS and the average loading of network components.

The resulting topology demonstrates coordination between both technologies to mitigate contingencies and redistribute loads. Overall, the solution highlights a selective and efficient integration of BESS resources within the transmission network.

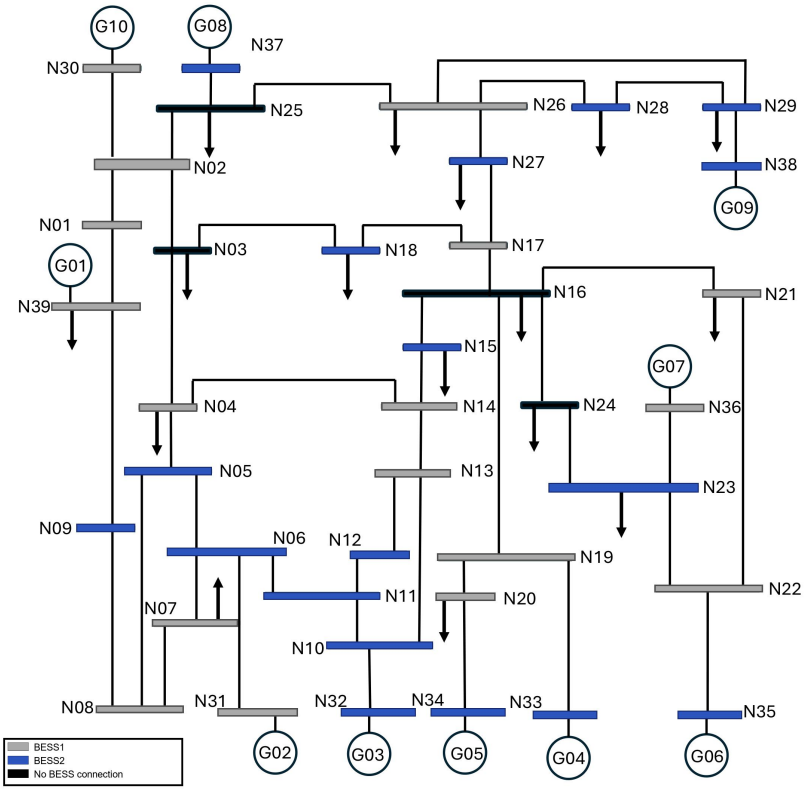


Figure 9. BESS locations in the unrestricted solution.

5.2. Restricted Scenario Analysis

Figure 10 shows the relationship between the maximum allowable investment cost and the fitness function obtained by the proposed reliability-oriented BESS planning framework. As the investment budget increases, the fitness value decreases rapidly at first and then more slowly, indicating diminishing reliability gains from additional storage capacity. This trend reflects the ability of larger BESS installations to supply energy during contingency events, thereby reducing the ENS caused by transmission component outages. Beyond a certain investment level, however, further increases in storage capacity provide only marginal improvements in system reliability, suggesting that the proposed methodology identifies an economically efficient trade-off between investment cost and reliability enhancement.

To quantitatively identify a representative cost–reliability compromise, the relative fitness gap of each restricted scenario with respect to the unrestricted solution was evaluated as $Gap_i = (F_i - F_{\text{unrestricted}})/F_{\text{unrestricted}} \times 100$. A maximum relative gap of 5% was adopted as the near-optimality criterion. Scenario C4 yielded a gap of 5.5% and therefore did not satisfy this criterion, whereas C5 achieved a gap of 4.19%. Consequently, C5 was the first and lowest-investment scenario within the adopted tolerance. Moreover, its investment of 299.87 MUSD is approximately 65.88% lower than the 878.76 MUSD required by the unrestricted solution. Therefore, C5 was selected as a representative compromise between investment cost and reliability performance and was subsequently used for the repeatability analysis.

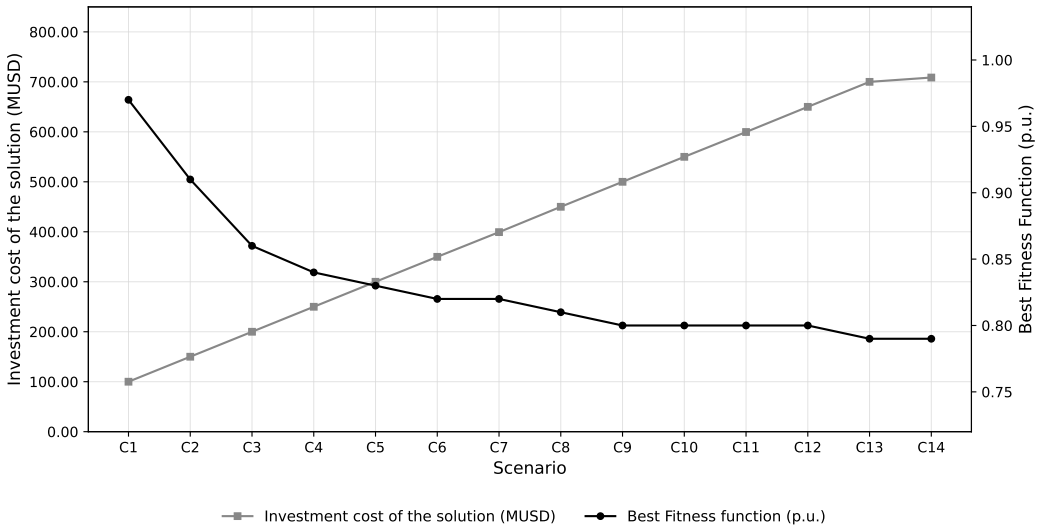


Figure 10. Investment costs and fitness values across budget scenarios.

Figure 11 shows the evolution of the incumbent fitness value for scenario C5. During the first 50 iterations, the value decreases from approximately 0.878 to 0.830 p.u., indicating rapid improvement in the feasible solutions. Between iterations 50 and 80, the decrease continues, though in smaller steps, until it settles around 0.828. From iteration 80 onward, the curve stays essentially flat, with a few minors isolated improvements near iterations 120, 135, and 145. This pattern indicates that the algorithm converged to a stable solution under the added constraints.

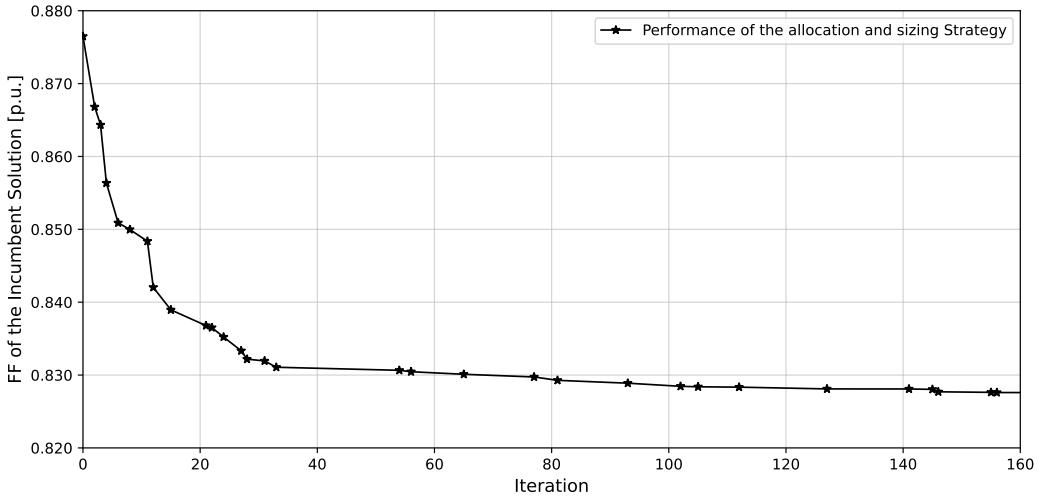


Figure 11. Fitness convergence in the restricted scenario.

Table 8 presents the BESS allocation and sizing obtained for case C5, showing the capacity assigned to BESS1 and BESS2 at each candidate bus. It also reports the total installed capacity for each storage technology and the corresponding investment cost, along with the overall investment required for the solution.

The restricted solution has a total installed BESS capacity of 338.66 MW, comprising 82.91% BESS1 and 17.09% BESS2, with a fitness value of 839,610.90 MWh/year. Buses 5 and 7 hold the largest capacities, at 79.54 MW and 79.69 MW, respectively. The lowest capacities are 1.00 MW at bus 35 (BESS1) and 1.07 MW at bus 10 (BESS2). Applying the assumed investment coefficients of 0.80 and 1.30 MUSD/MW yields investments of 224.62 and 75.24 MUSD, respectively. BESS1 therefore accounts for approximately 82.9% of the

installed BESS power capacity and 74.9% of the total investment. As in the unrestricted scenario, the optimized configuration also improves SAIDI and SAIFI, with both indices decreasing by approximately 13% relative to the reference case. The resulting allocation and sizing reflect the combined influence of the adopted technology costs, reliability parameters, and planning constraints.

Table 8. BESS allocation and rated power in the restricted solution.

BUS	BESS 1 Rated Power [MW]	BESS 2 Rated Power [MW]
3	0	1.10
4	0	1.34
5	79.54	0
6	1.22	0
7	79.69	0
9	1.22	0
10	0	1.07
13	0	1.12
16	0	43.00
20	0	1.29
21	0	2.21
22	0	1.16
23	22.61	0
24	0	1.36
25	0	1.64
27	0	1.22
28	24.94	0
30	1.20	0
33	33.08	0
34	0	1.37
35	1.00	0
38	36.28	0
Total BESS Power [MW]	280.78	57.88
Investment Cost [MUSD]	224.62	75.24
Total Investment Cost [MUSD]	299.87	
SAIDI Reduction [%]	13.76	
SAIFI Reduction [%]	13.11	
Fitness Function [MWh/year]	839,610.90	

Figure 12 shows the battery locations for the restricted case solution. Notably, Seventeen of the 39 buses have no BESS installed. Of the remaining 22 buses, 10 host BESS1 units and 12 host BESS2 units. These installations are distributed across buses near generators and load buses. The largest BESS1 capacities are concentrated at buses 5, 7, 33, and 38, while the largest BESS2 capacity is placed at bus 16. Bus 7 receives a high-capacity BESS in both the unrestricted and restricted solutions, suggesting that this location is favorable under the adopted planning conditions.

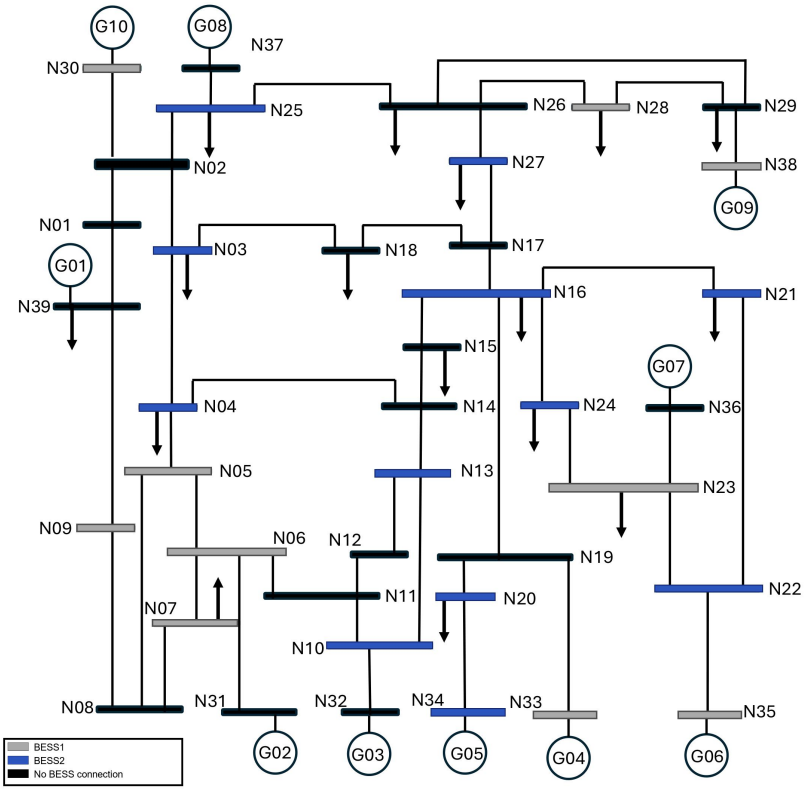


Figure 12. BESS locations in the restricted solution.

5.3. Performance of the Best Solution Analysis

This case examines the consistency of the MGWO results across ten independent runs for scenario C5, selected using the criterion described in Section 5.2.

Among the ten runs, run 6 produced the best solution, achieving the minimum objective-function value of 0.8213 p.u. Table 9 summarizes the optimization results obtained under a maximum investment budget of 300 MUSD. Across all runs, the proposed methodology converged to economically feasible solutions, with total investment costs ranging from 288 MUSD to 300 MUSD, demonstrating the capability of the optimization framework to satisfy the budget constraint imposed while maintaining competitive reliability performance.

Table 9. Results of the scenarios with a budget limit of 300 [MUSD].

Run	Investment Cost [MUSD]	Computation Time [h]	Fitness Function [p.u.]
1	299.94	2.70	0.8276
2	299.95	4.17	0.8262
3	299.98	3.64	0.8255
4	299.97	3.78	0.8251
5	288.80	4.04	0.8268
6	299.99	4.10	0.8213
7	299.98	3.96	0.8241
8	299.99	3.94	0.8300
9	299.98	4.14	0.8246
10	299.94	4.10	0.8256

Despite the stochastic nature of MGWO, the solutions exhibit a consistent deployment pattern. The optimization tends to allocate a limited number of high-capacity BESS1 units at strategically selected buses, while distributing a larger number of lower-capacity BESS2

units throughout the network. This behavior reflects the different technical and economic characteristics of the two storage technologies and indicates that the proposed planning framework exploits their complementary capabilities to maximize the reliability benefit within the available investment budget.

The 300 MUSD investment limit restricts the feasible combinations of BESS locations, technologies, and rated powers. Within this feasible set, the algorithm seeks to minimize the scenario-average annual ENS; investment enters as a constraint rather than as an objective or an ENS-reduction-per-cost criterion.

Figure 13 shows boxplots of the fitness values and installed capacities of each BESS technology. The final fitness values lie within a narrow range, between 0.8213 and 0.8300, with the median near 0.8256 and the central half of the data between 0.8247 and 0.8266. This indicates the algorithm converges to solutions of similar quality across nearly all runs, with no values markedly separated from the rest. The total installed BESS1 capacity ranges from approximately 250 to 355 MW, with a median near 290 MW. BESS2 capacity ranges from approximately 20 to 75 MW, with a median near 55 MW. BESS1 therefore accounts for most of the installed capacity across the ten runs.

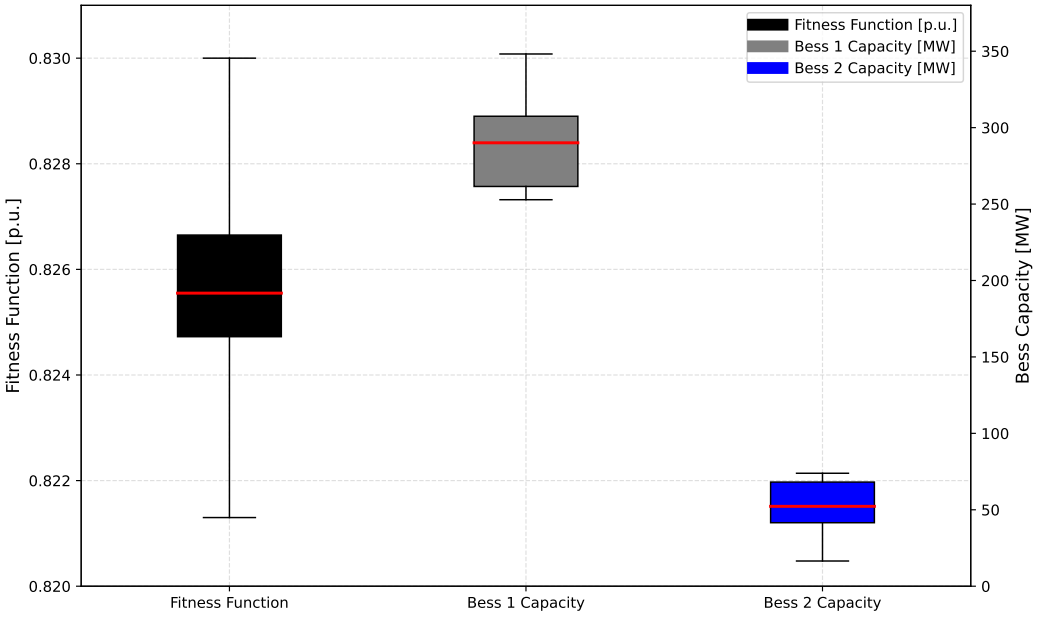


Figure 13. Distribution of final fitness values and installed BESS capacities across ten independent runs.

5.4. Comparison of BESS Planning Objectives

This section compares the proposed ENS-based strategy with strategies that minimize energy losses or the voltage deviation index (VDI). All cases use the same maximum investment budget of 300 MUSD, technology cost coefficients, and MGWO parameters reported in Table 6. Each resulting solution is evaluated using all three indicators. Component failure and repair parameters are considered exclusively in the reliability assessment used to calculate ENS. Energy losses and VDI are evaluated without probabilistic component failure and repair modeling. Energy losses are accumulated over uniform one-hour intervals. Table 10 summarizes the results.

The ENS-based solution achieves the lowest ENS among the three solutions, reducing it by approximately 0.94% relative to the loss-minimizing solution and 19.04% relative to the VDI-minimizing solution. This reliability benefit involves trade-offs: its energy losses are 8.86% higher than those of the loss-based solution, while its VDI is 9.58% higher than

that of the VDI-based solution. The installed capacities and technology mixes also differ: the VDI-, loss-, and ENS-based solutions allocate 356.6, 325.8, and 338.5 MW, respectively.

Table 10. Comparison of BESS planning objectives under a maximum investment budget of 300 MUSD.

Criterion	Investment Cost [MUSD]	Installed Capacity [MW] Total (Li-Ion/VRF)	ENS [MWh/Year]	Energy Losses [MWh]	VDI
VDI	299.95	356.6 (327.4/29.2)	1,037,116.80	402,283	0.07220
Losses	299.70	325.8 (247.9/77.9)	847,561.46	317,160	0.08167
ENS	299.87	338.5 (280.7/57.8)	839,610.90	345,276	0.07912

These results illustrate the trade-offs between reliability, energy loss reduction, and voltage regulation under a common investment limit. Among the three solutions, ENS-based planning achieves the lowest ENS, while loss- and VDI-based planning achieve the lowest values of their respective indicators. The comparison therefore highlights how the selected planning objective influences installed BESS capacity, technology mix, and the resulting balance between reliability and electrical performance.

6. Conclusions

6.1. Summary and Key Contributions

This work proposed an optimization framework for the allocation, sizing, and technology selection of BESS in transmission systems, integrating a Mixed Gray Wolf Optimizer (MGWO) with a stochastic reliability model of lines, transformers, and busbars. The fitness function was defined as the equally weighted average of annual ENS across single-generator-outage scenarios. Its evaluation combined hourly power flow calculations over a one-year horizon, representative weekday, Saturday, and Sunday demand profiles, and stochastic two-state component models. The results support reliability-oriented BESS planning under these assumptions, while full historical demand chronology and BESS energy depletion were not explicitly modeled.

The results obtained on the IEEE 39-bus system show that, without an investment limit, the algorithm allocated 499.36 MW of Li-ion BESS and 368.67 MW of VRF BESS. The resulting allocation included both technologies at different network locations, illustrating the technology mix obtained under the adopted planning and reliability assumptions.

Among the evaluated investment limits, 300 MUSD was the lowest budget yielding a fitness value within 5% of the result obtained without an investment limit. The corresponding solution required 299.87 MUSD, approximately 65.88% less than the unrestricted solution. This scenario was therefore selected as a representative cost–reliability compromise under the adopted tolerance.

Under a common investment limit of 300 MUSD, the ENS-based strategy achieved an annual ENS of 839,610.90 MWh/year, approximately 0.94% lower than the ENS obtained by minimizing energy losses and 19.04% lower than that obtained by minimizing voltage deviation. These reliability gains involved trade-offs: energy losses were 8.86% higher than in the loss-based solution, and voltage deviation was 9.58% higher than in the voltage-based solution. The comparison demonstrates how the planning objective influences BESS capacity, technology mix, and performance, without isolating the effect of component failure rate modeling alone.

6.2. Limitations and Future Work

The proposed methodology has several limitations that define the scope of the results. First, the BESS reliability model represents each storage system as an aggregated repairable

component with two mutually exclusive states: fully available and completely unavailable. Thus, the methodology accounts for BESS failures through the stochastic transition to the unavailable state, which represents a complete outage caused by a failure or maintenance event. However, this simplified representation does not explicitly model failures of individual BESS subsystems, such as battery modules, the power conversion system, the battery management system, cooling equipment, and auxiliary components. Furthermore, it does not represent derated operating conditions or partial-capacity states.

A relevant limitation is that the proposed methodology optimizes the active power capacity of the BESS units but does not explicitly determine their energy capacity or chronological state of charge. This simplification is particularly important because ENS is an energy-based reliability index and therefore depends on both the magnitude and duration of the power deficit. The current model implicitly assumes that sufficient stored energy is available to sustain the required BESS power injection during each evaluated contingency. Consequently, the reduction in ENS may be overestimated when the duration of an outage exceeds the actual discharge capability of the storage system. The reported capacities should therefore be interpreted as power capacity requirements rather than as a complete BESS design in MW and MWh.

Demand is represented using typical weekday, Saturday, and Sunday profiles. Although this approach reduces the computational burden, it may not capture short-term demand variability, chronological dependencies, extreme loading conditions, or correlations between demand and renewable generation. Another practical limitation is that the optimization algorithm determines continuous BESS power capacities, whereas commercially available storage systems are typically installed using standardized modules or discrete capacity blocks. Moreover, the present formulation focuses on minimizing ENS subject to an investment constraint and does not simultaneously consider other planning criteria, such as power losses, voltage performance, stability, and life-cycle costs.

Future research will extend the proposed methodology by incorporating multi-state or component-based BESS reliability models. These models will allow internal subsystem failures, partial-capacity states, derated operation, and dependencies among BESS components to be represented more realistically. The reliability model will also be coupled with chronological storage operation models incorporating energy capacity and state-of-charge constraints. Higher-resolution chronological demand and renewable generation scenarios will be considered to account for temporal variability and uncertainty.

Author Contributions: Conceptualization, J.G.M.-Q.; methodology, S.D.D.-P., J.I.S.-O. and J.G.M.-Q.; software, S.D.D.-P.; validation, S.D.D.-P., J.I.S.-O. and J.G.M.-Q.; formal analysis, R.P.G. and A.R.H.-O.; investigation, J.I.S.-O.; resources, J.G.M.-Q. and S.D.D.-P.; data curation, A.R.H.-O.; writing—original draft preparation, S.D.D.-P., J.G.M.-Q. and J.I.S.-O.; writing—review and editing, C.A.O.-H., J.G.M.-Q. and S.D.D.-P.; supervision, C.A.O.-H., A.R.H.-O. and R.P.G.; project administration, J.G.M.-Q.; funding acquisition, not applicable. All authors have read and agreed to the published version of the manuscript.

Funding: This research received no external funding. The Article Processing Charges (APCs) were funded by the authors.

Data Availability Statement: The data supporting the findings of this study are available from the corresponding author upon reasonable request.

Conflicts of Interest: The authors declare no conflicts of interest.

References

1. Salam, I.U.; Mazza, A.; Chicco, G. A conceptual view of grid weakness in transmission and distribution systems. *Electr. Power Syst. Res.* **2026**, *259*, 113193. [CrossRef]

2. Memari, M.; Karimi, A.; Vahidipour, S. Identifying critical transmission lines in power systems: A hybrid complex network and power flow methodology. *Electr. Power Syst. Res.* **2026**, *258*, 113105. [CrossRef]
3. Sudiarto, B.; Jufri, F.H.; Angkasa, F.F.; Widyanto, A.N.; Hudaya, C.; Husnayain, F.; Fitri, I.R.; Aryani, D.R.; Kim, J.S.; Samual, M.G.; et al. Battery technology for utility-scale battery energy storage system applications: A comparative review. *J. Energy Storage* **2026**, *149*, 120211. [CrossRef]
4. Mushid, F.C.; Khan, M.F. Battery Energy Storage for Ancillary Services in Distribution Networks: Technologies, Applications, and Deployment Challenges—A Comprehensive Review. *Energies* **2025**, *18*, 5443. [CrossRef]
5. Kapoor, A.; Rathoure, A.K.; Monica, M.; Chakraborty, A.; Tripathi, S.; Pal, D.B. Insights into advances in flexible lithium-ion battery energy storage systems toward sustainable applications. *Mater. Sci. Eng. B* **2025**, *318*, 118301. [CrossRef]
6. Sakib, S.; Hossain, M.B.; Zamee, M.A.; Hossain, M.; Habib, M.A. Role of battery energy storage systems: A comprehensive review on renewable energy zones integration in weak transmission networks. *J. Energy Storage* **2025**, *128*, 117223. [CrossRef]
7. Chen, P.; Cui, W.; Shang, J.; Xu, B.; Li, C.; Lun, D. Control Strategy of Multiple Battery Energy Storage Stations for Power Grid Peak Shaving. *Appl. Sci.* **2025**, *15*, 8656. Correction in *Appl. Sci.* **2026**, *16*, 381. [CrossRef]
8. Trivić, B.; Savić, A. Optimal Allocation and Sizing of BESS in a Distribution Network with High PV Production Using NSGA-II and LP Optimization Methods. *Energies* **2025**, *18*, 1076. [CrossRef]
9. Bakeer, A.; Chub, A.; Shen, Y.; Sangwongwanich, A. Reliability analysis of battery energy storage system for various stationary applications. *J. Energy Storage* **2022**, *50*, 104217. [CrossRef]
10. Okafor, C.E.; Folly, K.A. Optimal placement of BESS in a power system network for frequency support during contingency. *Energy Rep.* **2023**, *10*, 3681–3695. [CrossRef]
11. Alobaidi, A.H.; Khodayar, M.; Vafamehr, A.; Gangammanavar, H.; Khodayar, M.E. Stochastic expansion planning of battery energy storage for the interconnected distribution and data networks. *Int. J. Electr. Power Energy Syst.* **2021**, *133*, 107231. [CrossRef]
12. Albaaj, B.; Kaplan, O. Allocation of Battery System Storage with Uncertainty Renewable Energy Inside Modern Grids. In Proceedings of the 2025 13th International Conference on Smart Grid (icSmartGrid), Glasgow, UK, 27–29 May 2025; pp. 542–549. [CrossRef]
13. Xuan, A.; Shen, X.; Guo, Q.; Sun, H. A conditional value-at-risk based planning model for integrated energy system with energy storage and renewables. *Appl. Energy* **2021**, *294*, 116971. [CrossRef]
14. Yuan, Z.; Wang, W.; Wang, H.; Yildizbasi, A. A new methodology for optimal location and sizing of battery energy storage system in distribution networks for loss reduction. *J. Energy Storage* **2020**, *29*, 101368. [CrossRef]
15. Binini, G.M.; Munda, J.L.; Popoola, O.M. Optimal location, sizing and scheduling of distributed energy storage in a radial distribution network. *J. Energy Storage* **2024**, *94*, 112499. [CrossRef]
16. Wong, L.A.; Ramachandaramurthy, V.K.; Walker, S.L.; Taylor, P.; Sanjari, M.J. Optimal placement and sizing of battery energy storage system for losses reduction using whale optimization algorithm. *J. Energy Storage* **2019**, *26*, 100892. [CrossRef]
17. Bhattacharya, S.; Caruana, C.; Raute, R.; Micallef, A. Optimising the placement and sizing of a predefined number of battery energy storage systems on Distribution Networks. In Proceedings of the 12th IFAC Symposium on Control of Power and Energy Systems - CPES IFAC-PapersOnLine, Rabat, Morocco, 10–12 July 2024; Volume 58, pp. 38–43. [CrossRef]
18. Padhee, M.; Pal, A.; Mishra, C.; Vance, K.A. A Fixed-Flexible BESS Allocation Scheme for Transmission Networks Considering Uncertainties. *IEEE Trans. Sustain. Energy* **2020**, *11*, 1883–1897. [CrossRef]
19. Yuan, Z.; Wang, W.; Wang, H.; Yıldızbaşı, A. Allocation and sizing of battery energy storage system for primary frequency control based on bio-inspired methods: A case study. *Int. J. Hydrogen Energy* **2020**, *45*, 19455–19464. [CrossRef]
20. Motalleb, M.; Reihani, E.; Ghorbani, R. Optimal placement and sizing of the storage supporting transmission and distribution networks. *Renew. Energy* **2016**, *94*, 651–659. [CrossRef]
21. Sulaiman, M.H.; Mustaffa, Z.; Saari, M.M.; Jadin, M.S. A simulation-metaheuristic approach for finding the optimal allocation of the battery energy storage system problem in distribution networks. *Decis. Anal. J.* **2023**, *7*, 100208. [CrossRef]
22. Song, H.; Yang, P.; Li, L.; Lin, X.; Tian, X.; Wu, Z.; Zhang, X.; Peng, Z. Grid-Forming energy storage configuration method considering constraints of multiple renewable stations short-Circuit ratio. *Electr. Power Syst. Res.* **2027**, *263*, 113703. [CrossRef]
23. Li, L.; Song, H.; Wu, Y.; Li, H.; Lin, X.; Zhang, Y. Synchronization Stability of Microgrids Considering the Interaction Between GFL and AHO Inverters Under Current Limits. *IEEE Trans. Power Electron.* **2026**, *41*, 18870–18875. [CrossRef]
24. Xu, Z.; Tang, Z.; Chen, Y.; Liu, Y.; Gao, H.; Xu, X. Optimal robust allocation of distributed modular energy storage system in distribution networks for voltage regulation. *Appl. Energy* **2025**, *388*, 125625. [CrossRef]
25. Zhang, D.; Shafiullah, G.M.; Das, C.K.; Wong, K.W. Optimal Allocation of Battery Energy Storage Systems to Enhance System Performance and Reliability in Unbalanced Distribution Networks. *Energies* **2023**, *16*, 7127. [CrossRef]
26. Zhang, D.; Shafiullah, G.; Das, C.K.; Wong, K.W. Optimal allocation of battery energy storage systems to improve system reliability and voltage and frequency stability in weak grids. *Appl. Energy* **2025**, *377*, 124541. [CrossRef]
27. Parvar, S.S.; Nazaripouya, H. Optimal Operation of Battery Energy Storage Under Uncertainty Using Data-Driven Distributionally Robust Optimization. *Electr. Power Syst. Res.* **2022**, *211*, 108180. [CrossRef]

28. Pinheiro, L.V.; Ribeiro De Barros, T.; Willer De Oliveira, L.; Oliveira, J.G.; Soares, T.A.; Dias, B.H. Flexibility optimization from distributed storage resources under stochastic uncertainties. *Electr. Power Syst. Res.* **2026**, *254*, 112674. [CrossRef]
29. Fu, A.; Lekić, A.; Malamaki, K.N.D.; Kryonidis, G.C.; Mauricio, J.M.; Demoulias, C.S.; Palensky, P.; Cvetković, M. A stochastic simulation-based approach for sizing DRES penetration level and BESS capacity in distribution grids. *Int. J. Electr. Power Energy Syst.* **2024**, *161*, 110164. [CrossRef]
30. Galeela, M.; Kopsidas, K.; Chakravorty, D. Reliability Framework Integrating Grid Scale BESS Considering BESS Degradation. *Int. J. Electr. Power Energy Syst.* **2023**, *152*, 109228. [CrossRef]
31. Pijarski, P.; Belowski, A. Outage Rates and Failure Removal Times for Power Lines and Transformers. *Appl. Sci.* **2025**, *15*, 8030. [CrossRef]
32. Che, E.; Abeng, K.; Iweh, D.; Tsekouras, G.; Fopah Lele, A. The Impact of Integrating Variable Renewable Energy Sources into Grid-Connected Power Systems: Challenges, Mitigation Strategies, and Prospects. *Energies* **2025**, *18*, 689. [CrossRef]
33. Alsharif, H.; Jalili, M.; Hasan, K.N. Power system frequency stability using optimal sizing and placement of Battery Energy Storage System under uncertainty. *J. Energy Storage* **2022**, *50*, 104610. [CrossRef]
34. Qu, C.; Bang, R. European grid development modeling and analysis: Established frameworks, research trends, and future opportunities. *Discov. Energy* **2024**, *4*, 9. [CrossRef]
35. Breeze, P. Chapter 10—The Cost and Economics of Energy Storage. In *Power System Energy Storage Technologies*; Breeze, P., Ed.; Academic Press: Cambridge, MA, USA, 2018; pp. 85–89. [CrossRef]
36. Mirjalili, S.; Mirjalili, S.M.; Lewis, A. Grey Wolf Optimizer. *Adv. Eng. Softw.* **2014**, *69*, 46–61. [CrossRef]
37. Emary, E.; Zawbaa, H.M.; Hassanien, A.E. Binary grey wolf optimization approaches for feature selection. *Neurocomputing* **2016**, *172*, 371–381. [CrossRef]
38. Marín Quintero, J.; Uribe, J.A.; Bernal, O.; Orozco Henao, C. Optimal restoration algorithm for active distribution network considering island mode of the microgrids. *e-Prime-Adv. Electr. Eng. Electron. Energy* **2025**, *12*, 100976. [CrossRef]
39. Athay, T.; Podmore, R.; Virmani, S. A Practical Method for the Direct Analysis of Transient Stability. *IEEE Trans. Power Appar. Syst.* **1979**, *PAS-98*, 573–584. [CrossRef]
40. Liu, J.; Zhang, Z.; Zheng, X. Study on forecasting model of transmission line failure rate and outage time. *J. Phys. Conf. Ser.* **2023**, *2588*, 012017. [CrossRef]
41. Bao, Y.J.; Cheng, K.W.E.; Ding, K.; Wang, D.H. The study on the busbar system and its fault analysis. In Proceedings of the 2013 5th International Conference on Power Electronics Systems and Applications(PESA), Hong Kong, China, 11–13 December 2013; pp. 1–7. [CrossRef]
42. Otto, S. MRI Accreditation Framework for Energy Storage Resources. In Proceedings of the NEPOOL Joint Markets and Reliability Committees, Westborough, MA, USA, 16 December 2025; p. slide 7. Available online: https://www.iso-ne.com/static-assets/documents/100030/a04_a_car_sa_energy_storage_resource_modeling_and_accreditation_presentation.pdf (accessed on 21 October 2026).
43. Reichelt, F.; Müller, K. Assessment of the reliability of vanadium-redox flow batteries. *Eng. Rep.* **2020**, *2*, e12254. [CrossRef]
44. Mongird, K.; Fotedar, V.; Viswanathan, V.; Koritarov, V.; Balducci, P.; Hadjerioua, B.; Alam, J. *Energy Storage Technology and Cost Characterization Report*; Technical Report PNNL-28866; Pacific Northwest National Laboratory: Richland, WA, USA, 2019.

Disclaimer/Publisher's Note: The statements, opinions and data contained in all publications are solely those of the individual author(s) and contributor(s) and not of MDPI and/or the editor(s). MDPI and/or the editor(s) disclaim responsibility for any injury to people or property resulting from any ideas, methods, instructions or products referred to in the content.